Czech Technical University in Prague
Faculty of Nuclear Science and Physical Engineering

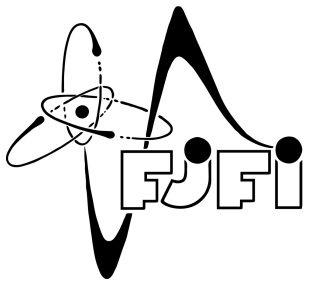

BACHELOR THESIS

MATHEMATICAL AND SOFTWARE TOOLS FOR THE ATLAS PIXEL DETECTOR ALIGNMENT

Pavel Ježˇ

Supervisor: Václav Vrba, CSc.

June 8, 2006

I would like to thank to my supervisor Václav Vrba for his valuable advices and inspiring discussions. I am also grateful to Richard Hawkings for introducing me to the Athena framework and for many useful discussions about reconstruction algorithms and offline analysis. Many thanks belong to my colleagues Lukáš Mašek, Petr Mikeš and Jan Valenta for the discussions about object-oriented programming and other computing issues. I am very thankful to Jiří Hořejší for answering my questions concerning particle physics theory. Finally I would like to thank Institute of Physics in Prague for allowing me to stay for several weeks in CERN where I gathered most of the material for this thesis.

Prohlášení

Prohlašuji, že jsem svou bakalářskou práci vypracoval samostatně a použil jsem pouze podklady uvedené v přiloženém seznamu.

Nemám závažný důvod proti užití tohoto školního díla ve smyslu §60 Zákona č. 121/2000 Sb., o právu autorském, o právech souvisejících s právem autorským a o změně některých zákonů (autorský zákon).

Declaration

I declare that I wrote my bachelor thesis independently and exclusively with the use of cited bibliography.

I agree with the usage of this thesis in the purport of the Act 121/2000 (Copyright Act).

Praha, June 8, 2006 Pavel Jež

Název práce:
Matematické a softwarové nástroje pro justaci pixelového detektoru ATLAS

Autor: Pavel Jež

Obor: Matematické inženýrství

Druh práce: Bakalářská práce

Vedoucí práce: Václav Vrba, CSc. Katedra fyziky, Fakulta jaderná a fyzikálně inženýrská, České vysoké učení technické v Praze

Abstrakt: V úvodních částech práce je popsán současný stav fyziky částic po stránce teorie i experimentu. V první kapitole je stručně načrtnut standardní model částicové fyziky. Důraz je kladen na experimentální ověřování jeho předpovědí. Na konci je probírán počet volných parametrů a možná rozšíření. Další kapitola popisuje urychlovačový komplex v CERNu, především LHC a experimenty na něm. Představují se hlavní cíle a očekávání fyzikálního programu na LHC. Třetí kapitola obsahuje popis detektoru ATLAS a jeho subdetektorů. Ve čtvrté kapitole je vlastní výzkumný přínos autora. Je věnován metodickým, softwarovým a matematickým prostředkům pro stanovení přesné pozice subdetektorů v celém detekčním systému ATLAS, které je nezbytné pro řešení plánovaného výzkumného programu popsaného v první a druhé kapitole. Konkrétně se zabývá tvarovými deformacemi pixelových detektorů. V práci je popsána koncepce iterativní justace detektorů založená na optimalizaci drah částic a pozic zásahů v detekčních čidlech.

Klíčová slova: standardní model, ATLAS, justace, pixelové detektory, offline analýza.

Title: **Mathematical and Software Tools for the ATLAS Pixel Detector Alignment**

Author: Pavel Ježˇ

Abstract: The opening sections of this thesis describe a contemporary state of high energy physics, both from the view of theory and experiment. In the first chapter the basic concepts of the Standard Model are briefly outlined. Emphasis is put on the experimental verification of its predictions. Number of free parameters and possible extensions are discussed at the end. Next chapter describe CERN accelerator complex and LHC experiments in particular. It shows the main goals and expectations of LHC physics programme. The third chapters contains description of the ATLAS detector and all its subdetectors. Author's original research contribution is in the fourth chapter. It is devoted to methodical, software and mathematical tools for the determination of the precise position of subdetectors in the whole ATLAS detection system, which is essential for the research programme described in the first and second chapter. In particular, it treats the ATLAS Inner Detector misalignment and pixel modules shape distortions. The thesis describe the concept of the iterative detector alignment based on the optimization of particles tracks and position of hits in detective modules.

Key words: Standard Model, ATLAS, pixel detector, alignment, offline analysis.

Contents

Chapter 1

Standard Model

1.1 Way to Standard Model

Although the idea that all matter is composed from tiny indivisible particles is quite old (Democritus and Leucippus, 5th century BC), it had to wait for more than two millennia for some experimental support. Inspired by his chemical discoveries, J. Dalton proposed that each element is made from indivisible atoms of one type. Few decades later D. Mendeleev noticed that some properties of elements sort by atomic weight exhibit apparent periodicity. This was the first indication of the existence of some atomic structure. The first subatomic particle, electron, was discovered by J. J. Thomson before the end of the 19th century.

In the beginning of the 20th century Rutherford, Geiger and Marshden carried out a series of scattering experiments which proved the existence of the atomic nucleus. Since then the vast majority of subnuclear experiments modelled themselves upon Rutherford, only using higher energies and more precise detectors.

A few years later scattering experiments showed that the immediate environment of the nucleus is governed by other forces than electromagnetism or gravitation: the concept of strong interaction was born. Meanwhile it became generally accepted, that there also exist fourth force, responsible for β-decay - now it is called weak.

In 1932 Chadwick discovered neutron. Shortly afterwards, Heisenberg proposed that atomic nuclei are composed from protons and neutrons, but he was not able to figure out the nature of force which holds nucleus together. He thought that this interaction works by the means of exchanging electrons. This also explained electrons emerging out of nucleus during β-decay.

In 1933 Fermi published his theory of weak force - cause of a long known β-

decay, which became the first successful theory of intranuclear force besides the electromagnetism. It was formulated in a language of the quantum field theory, so the particles were created and destroyed as a consequence of very notion of the quantum field. The assumption of electrons present in nuclei was therefore no longer necessary.

Couple of years later Yukawa realized the relation between the range of the force and the mass of the intermediating particle. Hence, he supposed, that the strong interaction is mediated by particles which have mass about two hundred times that of electron and have charge plus or minus that of electron. Nevertheless, Yukawa theory was not charge invariant, as it described the interaction between proton and neutron only.

Later the experimental data showed that the strong interaction is charge invariant. This fact was incorporated into the theory in the following way: proton and neutron were considered to be members of a doublet, in analogy with two spin states of particles with spin 1/2. So the new internal degree of freedom of the nucleon was introduced, now called isospin. This property was supposed to be invariant under strong interaction, which led to the extension of the Pauli exclusion principle by adding a new variable describing the state of nucleon.

The concept of isospin is very similar to that of spin. The operator of isospin satisfies angular commutation relations

$$\left[\hat{T}_i, \hat{T}_j\right] = i\varepsilon_{ijk}\hat{T}_k \quad \text{and} \quad \left[\hat{\mathbf{T}}^2, \hat{T}_j\right] = 0$$

where $\hat{\mathbf{T}}$ is the (vector) operator of isospin and $\hat{T}_i$ are its components. From the above relations it can be derived that the eigenvalues of the operator $\hat{\mathbf{T}}^2$ take form $j(j+1)$, where j is a nonnegative integer or half an odd positive integer and the eigenvalues of $\hat{T}_3$ are numbers $j, j-1, \ldots, -j+1, -j$. It is common to say that particle has isospin j while it is at the state corresponding to eigenvalue $j(j+1)$ of $\hat{\mathbf{T}}^2$.

Because for given value of isospin $T = j$ there is $2T+1$ possible values of T_3 (without hat it is just a symbol for the third value of isospin, not an operator), a multiplet with isospin T has $2T+1$ members (e.g. nucleon doublet has isospin 1/2, triplet $\pi^{\pm}$, π^0 has isospin 1). Multiplet members differs in the third component of isospin (like particles with spin 1/2 can have its third component either +1/2 or -1/2). The particle with most positive charge is assigned j as its T_3 value, while $T_3 = -j$ is assigned to the most negative particle. Table 1.1 shows isospin of chosen particle multiplets.

Table 1.1: Isospin values

particle	T	T_3
p	1/2	+1/2
n	1/2	-1/2
π^+	1	+1
π^0	1	0
π^-	1	-1
η	0	0

To make the Yukawa theory charge (i.e. isospin) invariant, a neutral companion of charged Yukawa mesons was introduced. This way the concept of isospin was extended also on this triplet of intermediating mesons.

As the number of known particles increased (muon was discovered in late 1930s, pions (Yukawa particles) - $\pi^{\pm}$ and π^0 were founded in 1940s), they were divided into two groups: strongly interacting particles (nucleons, pions) were called hadrons, while the others (electron, muon) were called leptons. The first group was further divided into baryons (i.e. particles that have an odd number of protons and antiprotons among decay products - for example nucleons) and mesons (the rest - for example pions).

In the end of 1940s and in the beginning of 1950s there were discovered some particles which decayed (among others) into less massive hadrons, but this decay was much slower than it was expected for the strong interaction, indicating that the decay is mediated by the weak interaction. Because no known conservation law prevented strong decay of this particles (called "strange" particles), shortly after this discovery Nishijima proposed, that this could be explained in a terms of a new quantum number, which was later named strangeness. This was another property conserved by the strong interaction but violated by the weak one. The relation between isospin, strangeness, charge and baryon number (1 for baryons, -1 for antibaryons, 0 for others) was formulated in the famous Gell-Mann Nishijima relation:

$$Q = T_3 + \frac{B+S}{2} \tag{1.1}$$

Q stands for charge, T_3 for the third component of isospin, B for baryon number and S for strangeness. It could be rewritten using hypercharge $Y \equiv B + S$, which is twice the average charge of the multiplet. This is a direct consequence of formula

1.1, because the average third component of isospin of a given multiplet is always zero.

Since discoveries of the new particles did not stop, it was less and less probable that all of them would be elementary, so various explanation od particle structure appeared. The most important of them was proposed by Murray Gell-Mann who supposed, that *all* hadrons are made out of some three basic components (which he did not specify). Because of possible representations of $SU(3)$ group (i.e. approximate symmetry to the interchange of this three basic components) Gell-Mann supposed, that particles can be organized into decuplets, octets and singlets. He indeed created a multiplets from particles sharing the same spin and baryon numbers. Figure 1.1[1] shows his meson octet with spin 0, figure 1.2 shows baryon octet with spin 1/2, and figure 1.3 shows his baryon decuplet with spin 3/2. Gell-Mann called this model Eightfold way. Because it predicted particle which was never before observed, but was discovered a few years later (Ω^-), Eightfold way was considered to be a great success. The important consequence of this model is, that pions are no longer privileged in any way, so that they could not mediate the strong interaction.

In January 1964 Murray Gell-Mann and George Zweig independently postulated the existence of 3 particles which have fractionate baryon number and fractionate charge and together they are the constituents of all hadrons. These particles were called quarks up (u), down (d) and strange (s). They were supposed to form the fundamental triplet of some $SU(3)$ symmetry group. The multiplets of Eightfold way were then viewed as different representations of this symmetry group. Although three more quarks were later added to this model and the group of symmetry was changed, the basic idea of hadrons made of quarks remained one of the most important components of the Standard Model. It also became clear, that the quantum number strangeness is just the number of s-quarks, therefore we can say, that strong interaction does not change the species of the quark ("flavour"), while the weak interaction does.

Today we suppose that all matter is composed from 24 elementary particles: 6 leptons, 6 antileptons, 6 flavours of quarks and 6 flavours of antiquarks - see table 1.2. According to their mass they are divided into three generations of matter. Practically all observable mass belongs to the first generation, because particles from the second and third family are highly unstable and quickly decay into less massive particles.

Three quarks together form baryons (like n or p), while quark-antiquark couples form mesons (e.g. π). Leptons and quarks are all fermions (i.e. they have half

[1]Pictures 1.1, 1.2 and 1.3 were taken from [6]

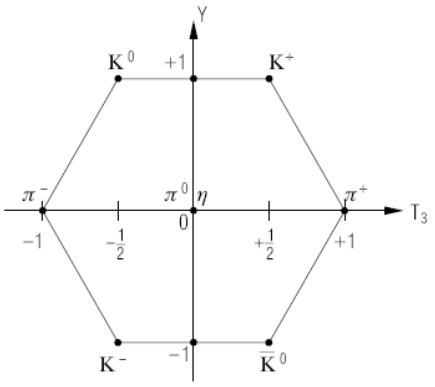

Figure 1.1: Mesons with spin 0

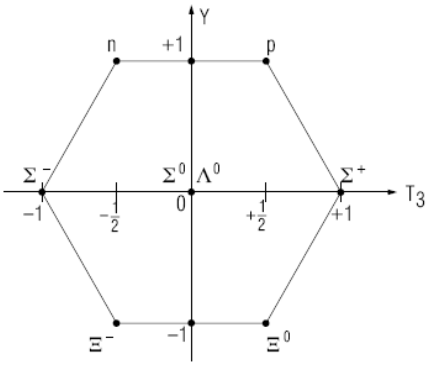

Figure 1.2: Baryons with spin 1/2

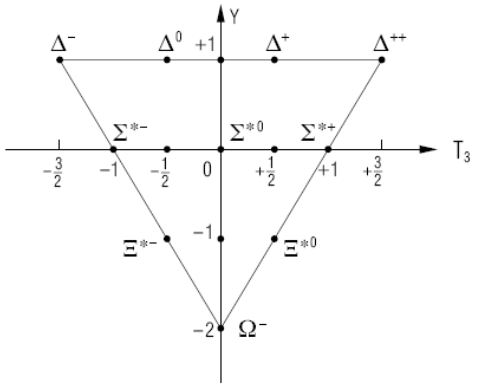

Figure 1.3: Baryons with spin 3/2

integer spin and obey the Pauli exclusion principle). Although leptons are directly observable, quarks are confined in mesons and baryons.

The quark model is very successful in describing the particle world. If we restricts ourselves to the baryons made from the tree lightest quarks (u, d, and s) only, there are $3^3 = 27$ possible states. Only one of them is fully antisymmetric (with respect to the interchange of quarks):

$$uds + dsu + sud - usd - sdu - dus$$

Note that it depends on the ordering of quark wavefunctions, which is a natural consequence of the introduction of an intrinsic quark property called colour charge

(see below). In a similar way we can construct fully symmetrical decuplet of baryon states, and two octets with mixed symmetry properties. We can also construct mesons states: there are $3^2 = 9$ of them and we can form a singlet and octuple out of them. This way we can construct the famous multiplets of Gell-Mann's Eightfold Way. All particles predicted by this model have been found and no others. If we add another three quarks, we can predict a lot of new particles, nevertheless, most of them have not been observed yet, probably because of the high mass and instability of other three quarks.

Particles interact through the four fundamental forces of nature. The gravitation is universal and a long range force. That is why it is dominant on an astronomical scale. However, it negligible on laboratory scale, so it is not incorporated in the Standard Model.

The electromagnetic interaction is also of a long range, but it is not universal - it affects only charged particles. Compared with others it is the second strongest force. Its effects on the classical scale are perfectly described by the Maxwell equations. The quantum version of theory of electromagnetism is called Quantum Electrodynamics - QED. In the 1960s QED was merged with the theory of a weak force - the Standard Model of electroweak interaction was created. Electromagnetic interaction conserves parity (symmetry under spatial inversion) and it is mediated by massless and neutral photons.

The weak interaction has a short range (about 10^{-18} m - 1000 times smaller than atomic nucleus). However it affects all quarks and leptons and it is the only interaction that changes flavour of quarks. The most common effect caused by the weak interaction is β decay. It was first described by Fermi's theory of four-fermion interaction, but this theory was insufficient for higher energies. Today we use the electroweak theory by Glashow, Weinberg and Salam which states that weak interaction is mediated by three massive bosons: W^+ boson has a positive charge, W^- is negative and the Z boson is neutral. All of them were experimentally observed and their mass was in perfect agreement with the values predicted by the GWS Standard Model.

The strong interaction has also short range - about 10^{-15} m, however it acts only on particles with a "colour charge" - this is an intrinsic property that each quark carries beside electrical charge (sometimes it is called "strong charge"). There are three possible types of colour charge. The particles interact by exchanging gluons. We suppose that there are eight types of this intermediating particles, each massless and each carrying different colour charge.

Objects made from quarks - hadrons - are colour-neutral but interact due to residual strong interaction between their components (similarly to the neutral atoms

Table 1.2: Elementary Particles

	First generation	Second generation	Third generation	Electrical charge
quarks	u-up	c-charm	t-top	+2/3
	d-down	s-strange	b-bottom	-1/3
leptons	e-electron	μ-muon	τ-tauon	-1
	ν_e - e-neutrino	ν_μ - μ-neutrino	ν_τ - τ-neutrino	0

forming molecules) - this force is responsible for the existence of atomic nucleus. The residual strong force is mediated by mesons, i.e. quark-antiquark bounded states.

Another interesting property of the strong interaction is the practical impossibility to isolate quarks and gluons - when we try to do this, the energy of the colour field binding them together increases until the new pair of quark-antiquark is created. Finally all quarks and antiquarks form hadrons which then emerge from the reaction. Therefore we say, that under normal conditions the quarks are confined inside hadrons. However it is supposed, that deconfined quark states exists in an extreme phase of matter called quark-gluon plasma.

All this phenomena are subject of the Quantum Chromodynamics (QCD) which was formulated in 1970s by Gross, Wilczek and Politzer. Both QCD and GWS Standard Model are gauge quantum field theories, so in the next sections the basic ideas of this type of theory will be introduced.

1.2 Introduction to Quantum Field Theory

1.2.1 Quantum Mechanics

Quantum mechanics was formulated during the first half of the 20th century by M. Planck, A. Einstein, N. Bohr, W. Heisenberg, E. Schrödinger, M. Born, J. von Neumann, P. Dirac, W. Pauli and many others. It is able to precisely describe the phenomena which cannot be explained by Newtonian mechanics of Maxwell electromagnetism - for example the very existence of electrons in the electron cloud around the atom nucleus.

In Hamiltonian mechanics the phase space of an n-dimensional system is $\mathbb{R}^{2n}$. Each vector of this space represents a physical state of a particle - n coordinates of

the position and n coordinates of the momentum. The observable quantities (mostly called observable for short) like energy, angular momentum, etc. are represented as real functions of generally $2n$ variables - for instance $E = \sum_{i=1}^{n} p_i^2/(2m)$. The dynamics of a classical system is given by the Hamiltonian (that is also one of the observables): The time-dependence of an observable A is given by

$$\frac{\mathrm{d}A(t)}{\mathrm{d}t} = \{A(t), H\} \tag{1.2}$$

where we suppose that A is not explicit function of time and the $\{\}$ denotes Poisson bracket. Because the state is characterized by the position and momentum, that are also observables on Hamilton phase space, the time-dependance of a given state can be obtained by substituting $A \to q$ and $A \to p$ in (1.2). We would of course get nothing else than well known Hamilton equations.

However, the mathematical structure of quantum mechanics is quite different. The state is represented by a vector in a complex separable Hilbert space (i.e. it has inner product and it is complete in a norm generated by the inner product). For example one n-dimensional particle lives in $L^2(\mathbb{R}^n, \mathrm{d}^n x)$, therefore the state of a particle in three dimensions is represented by a (class of) complex, quadratically integrable function(s) of n variables with unit norm. The last inquiry is necessary because of physical interpretation of the states: if a particle is in a state $\psi(x)$, then the probability density of finding the particle at a point x is $|\psi(x)|^2$. The integral from the probability density over whole space (=1) is then nothing else than the second power of the L^2 norm of ψ.

The observables are represented by linear self-adjoint operators on respective Hilbert spaces. The assignment of operators to the classical observables (i.e. functions on phase space) is called canonical quantization. Natural requirement on such a procedure is that it should not change the relations between the observables. This is however complicated by a fact that operators (in contrast to the functions) do not generally commute. Therefore we use Poisson brackets of the classical observables to define commutators of the respective operators. The assignment is

$$\{a, b\} \to -\frac{i}{\hbar}\left[\hat{A}, \hat{B}\right] \tag{1.3}$$

where a and b are classical observables and $\hat{A}$, $\hat{B}$ are operators on Hilbert space. The fundamental commutator is that of position and momentum:

$$\left[\hat{Q}_i, \hat{P}_j\right] = i\hbar\delta_{ij} \tag{1.4}$$

This is satisfied by

$$\hat{Q}\psi(x) = x\psi(x) \qquad \hat{P}\psi(x) = -i\frac{\mathrm{d}\psi(x)}{\mathrm{d}x}$$

It is worth noting that operator $\hat{P}$ is not defined on whole Hilbert space (the requirement of being self-adjoint). Other operators must satisfy (among others) this conditions:

- its commutation relations satisfy (1.3)
- the operator is self-adjoint
- the operator should be the same function of $\hat{Q}$ and $\hat{P}$ as in the classical case - this is important to achieve classical limit, but some quantum mechanical observables do not have classical analogy
- the operator has some physical relevance, i.e. it could be used to predict outcome of the experiment

The dynamics is again given by the Hamiltonian $\hat{H}$ - it is an observable and therefore self-adjoint linear operator on the Hilbert space. The relation for time-dependence of states is called Schrödinger equation:

$$i\frac{\mathrm{d}}{\mathrm{d}t}\psi_t = \hat{H}\psi_t \tag{1.5}$$

where ψ_t denotes the state at a time t.

1.2.2 Quantum Field Theory

Although quantum mechanics is a very successful theory, it has several flaws. From the construction is obvious that QM is a non-relativistic theory - it treats time and space separately and, moreover, it is a fixed particle theory, so it cannot describe such phenomena like excitation (an atom changes to atom at lower energy state and a photon). Therefore the quantum field theory was introduced.

In case of QM we quantized the motion of a single particle using the relations that came from the Hamiltonian formulation of classical mechanics. In QFT we quantize a field. In practice this means that instead of finding operators of position and momentum and subsequently constructing other operators from them, we

have a space-time parameterized operator (field) $\hat{\phi}(x,t)$ and all other operators are constructed from it.

We will now quantize the real scalar field (Klein-Gordon field). This is described by Klein-Gordon equation

$$(\Box + m^2)\phi = 0, \tag{1.6}$$

where $\phi = \phi(t, \mathbf{x})$, i.e. classical field. This relation could be derived using Euler-Lagrange equations (cf. [1] or [2]) from Lagrangian

$$\mathscr{L} = \frac{1}{2}(\partial_\mu \phi)(\partial^\mu \phi) - \frac{m^2}{2}\phi^2$$

where $\partial_\mu = (\partial_0/c, \nabla)$. The general solution of (1.6) is the superposition of plane waves:

$$\phi(t,\mathbf{x}) = \int \frac{\mathrm{d}^3\mathbf{k}}{(2\pi)^{3/2}\sqrt{2\omega_\mathbf{k}}} \left(a_\mathbf{k} \exp(i\mathbf{k}\cdot\mathbf{x} - \omega_\mathbf{k} t) + a^*_\mathbf{k} \exp[-(i\mathbf{k}\cdot\mathbf{x} - \omega_\mathbf{k} t)]\right)$$

where

$$\omega_\mathbf{k} = \sqrt{m^2 + \mathbf{k}^2}$$

Now we can calculate momentum

$$\pi(t,\mathbf{x}) = \frac{\partial \mathscr{L}}{\partial \dot{\phi}} = \dot{\phi}$$

The quantization means that we (similar to the previous section) postulate some commutation relation. In this case it is

$$\left[\hat{\phi}(t,\mathbf{x}), \hat{\pi}(t,\mathbf{y})\right] = i\hbar\delta(\mathbf{x}-\mathbf{y}) \tag{1.7}$$

This relation is satisfied by the above written solution of the Klein-Gordon equation, provided we are treating the coefficients of the Fourier expansion as an operators $\hat{a}_\mathbf{k}$ and $\hat{a}^\dagger_\mathbf{k}$. The relation (1.7) implies that

$$[\hat{a}_\mathbf{i}, \hat{a}_\mathbf{j}] = 0 \qquad [\hat{a}^\dagger_\mathbf{i}, \hat{a}^\dagger_\mathbf{j}] = 0 \qquad [\hat{a}_\mathbf{i}, \hat{a}^\dagger_\mathbf{j}] = \delta(\mathbf{i}-\mathbf{j})$$

This operators could be interpreted as creation and annihilation operators (see below), therefore we have constructed a theory with varying number of particles.

We can also construct an operator of energy - a Hamiltonian:

$$\hat{H} = \int (\hat{\pi}\partial_t\hat{\phi} - \hat{\mathscr{L}})\mathrm{d}^3\mathbf{x} = \int \mathrm{d}^3\mathbf{k}\omega_\mathbf{k}\hat{a}^\dagger_\mathbf{k}\hat{a}_\mathbf{k}$$

From this relation it is obvious that creation and annihilation operators behave in a similar way to the "ladder" operators of quantum harmonic oscillator.

QFT operators also acts on a separable Hilbert space, though a very special one. Let $\mathscr{H}$ be a Hilbert space of one-particle states. Then the tensor product $\mathscr{H}^{(n)} = \mathscr{H} \otimes \cdots \otimes \mathscr{H}$ denotes a Hilbert space of n particles and $\mathscr{H}^{(0)} = \mathbb{C}$ is a Hilbert space of no particles, so-called vacuum, or ground state. Now we can define Fock space (cf. [27]) $\mathscr{F}(\mathscr{H})$ as a direct sum

$$\mathscr{F}(\mathscr{H}) = \sum_{n=0}^{\infty}{}^{\oplus} \mathscr{H}^{(n)}$$

This is a Hilbert space of an arbitrary number of particles.

For the reasons of brevity, suppose we have a purely bosonic system (for fermionic system we would only have to take care that maximum number of particles in one state is one, do the antisymmetrization instead of symmetrization and replace all commutators with anticommutators). All possible states of this system form a Fock space. One particular state will look like

$$\frac{1}{\sqrt{3}}\left(|\phi_2\rangle|\phi_4\rangle|\phi_4\rangle + |\phi_4\rangle|\phi_2\rangle|\phi_4\rangle + |\phi_4\rangle|\phi_4\rangle|\phi_2\rangle\right) \equiv |0,1,0,2,0,0,\dots\rangle \tag{1.8}$$

meaning that there is one particle in the first excited state, two in the second excited state and no particles in other states. Equation (1.8) shows how are vectors from the Fock space constructed: $|\phi_i\rangle$ is properly normalized vector from one-particle Hilbert space corresponding to the i-th energy state (i.e. $(i-1)$-th excitation). All energy states together form an orthonormal basis of corresponding Hilbert space. Vectors of type $|\phi_i\rangle|\phi_j\rangle|\phi_k\rangle$ form an orthonormal basis of a space $\mathscr{H}^{(3)}$ because basis of a direct product of Hilbert spaces can be formed from the all possible products of base vectors of the original spaces. Last step is symmetrization - bosons are undistinguishable particles - and normalization. All these are just an technical obstructions which are hidden in the elegant form on the right side of (1.8).

The latter notation allow us to show effects of annihilation operator $\hat{a}_i$ and creation operator $\hat{a}_i^\dagger$. They work in a following way - they destroy or create particle in a state i:

$$\begin{aligned} a_i|\dots,N_{i-1},N_i,N_{i+1},\dots\rangle &= \sqrt{N_i}|\dots,N_{i-1},N_i-1,N_{i+1},\dots\rangle \\ a_i^\dagger|\dots,N_{i-1},N_i,N_{i+1},\dots\rangle &= \sqrt{N_i+1}|\dots,N_{i-1},N_i+1,N_{i+1},\dots\rangle \end{aligned} \tag{1.9}$$

To sum up, to construct a proper field theory, we have to find operators which satisfy (1.7), usually by finding a solution of an equation for a classical field. From

Fourier expansion of this solution we will (usually) get an annihilation and creation operator, which are crucial in particle interpretation. Other operators can be constructed from the generalized coordinate ϕ and generalized momentum π using the relations of the classical physics. However, in practice we are not able to solve QFT equations analytically, so to obtain some experimentally verifiable results from QFT Lagrangians, it is often necessary to use perturbation theory and Feynman path integrals. Last remark to the QFT in general is, that it does not stand on such a firm mathematical footing as QM - there has been proposed several sets of axioms, but it is extraordinary difficult to show that some realistic QFT satisfies them.

1.3 Abelian gauge theories

Inhomogeneous Maxwell equations can be written in a familiar covariant form

$$\partial_\mu F^{\mu\nu} = j^\nu \tag{1.10}$$

where electromagnetic tensor $F^{\mu\nu}$ is a 4-dimensional curl

$$F^{\mu\nu} = \partial^\mu A^\nu - \partial^\nu A^\mu \tag{1.11}$$

and $j^\nu = (\rho, \mathbf{j})$ is 4-current. Note that for $A^\mu = (\phi, \mathbf{A})$ is equation (1.11) equivalent to the homogenous Maxwell equations.

However, the 4-potential A^μ does not specify the electromagnetic field uniquely. The physics remains unchanged under a gauge transformation

$$A^\mu \to A^\mu + \partial^\mu \chi$$

where χ is an arbitrary scalar function. We showed that Maxwell equations of electromagnetism imply the existence of the symmetry of their solution. The symmetry takes form of a local gauge invariance (χ can have different values at different points).

But, on the other hand, can the gauge symmetry imply dynamics? Let us have the Lagrangian of a free Dirac field (i.e. particles with spin 1/2)

$$\mathscr{L}_0 = i\bar{\psi}\gamma^\mu \partial_\mu \psi - m\bar{\psi}\psi \tag{1.12}$$

where ψ is bispinor (i.e. 4-component) field variable and γ^μ are 4×4 matrices

$$\gamma^0 = \begin{pmatrix} 0 & 1 \\ 1 & 0 \end{pmatrix}, \quad \gamma^i = \begin{pmatrix} 0 & -\sigma^i \\ \sigma^i & 0 \end{pmatrix}$$

where σ^i are Pauli 2×2 matrices

$$\sigma_1 = \begin{pmatrix} 0 & 1 \\ 1 & 0 \end{pmatrix}, \quad \sigma_2 = \begin{pmatrix} 0 & -i \\ i & 0 \end{pmatrix}, \quad \sigma_3 = \begin{pmatrix} 1 & 0 \\ 0 & -1 \end{pmatrix}$$

and $\bar{\psi}$ denotes Dirac adjoint which is defined as follows:

$$\bar{\phi} = \phi^\dagger \gamma_0$$

Bispinor ψ can be written in a form

$$\psi = \begin{pmatrix} \phi_R \\ \phi_L \end{pmatrix} \tag{1.13}$$

Right-handed spinor (i.e. 2-component complex "vector") ψ_R transforms like

$$\psi_R = \begin{pmatrix} \xi_1 \\ \xi_2 \end{pmatrix} \to \exp\left[i\left(\frac{\boldsymbol{\sigma}}{2} \cdot \boldsymbol{\theta} - i\frac{\boldsymbol{\sigma}}{2} \cdot \boldsymbol{\phi}\right)\right] \begin{pmatrix} \xi_1 \\ \xi_2 \end{pmatrix}$$

while left-handed ψ_L transforms like

$$\psi_L = \begin{pmatrix} \eta_1 \\ \eta_2 \end{pmatrix} \to \exp\left[i\left(\frac{\boldsymbol{\sigma}}{2} \cdot \boldsymbol{\theta} + i\frac{\boldsymbol{\sigma}}{2} \cdot \boldsymbol{\phi}\right)\right] \begin{pmatrix} \eta_1 \\ \eta_2 \end{pmatrix}$$

Matrices $\boldsymbol{J} = \boldsymbol{\sigma}/2$ and $\boldsymbol{K} = \pm i\boldsymbol{\sigma}/2$ each generate group $SU(2)$. The first stands for spatial rotation with parameter $\boldsymbol{\theta}$, the latter stands for Lorentz "boost". Together they form two inequivalent (one with $\boldsymbol{K} = i\boldsymbol{\sigma}/2$, the other with $\boldsymbol{K} = -i\boldsymbol{\sigma}/2$) representations of the Lorentz transformation group. It has six parameters - three angles $\boldsymbol{\theta}$ (meaning the angles of rotation) and three angles $\boldsymbol{\phi}$ (related to the velocities in a following way $\gamma = \cosh\phi$ and $\gamma\beta = \sinh\phi$). More information about spinors, their construction and their transformation can be found in a book [2].

If we substitute Lagrangian (1.12) into Euler-Lagrange equation we get well known Dirac equation

$$(i\gamma^\mu \partial_\mu - m)\psi = 0$$

The Lagrangian is clearly invariant under global transformation

$$\psi' = e^{i\Lambda}\psi; \quad \bar{\psi}' = e^{-i\Lambda}\bar{\psi} \tag{1.14}$$

where Λ is a real constant. Noether's theorem now says that if Lagrangian is invariant under some group of transformations, then there exist one or more conserved

quantities. In this case our group of transformations is $U(1)$, i.e. rotation in a complex plane, and the respective conserved quantity is

$$J_\mu = \bar{\psi}\gamma_\mu\psi$$

Transformation (1.14) means that all points make the same rotation at the same time. This, however, does not follow the relativistic principle because the information about how to rotate cannot propagate more quickly than light. So let us suppose, that Λ is an arbitrary function of a space-time $\Lambda = \Lambda(x^\mu)$. Thus we got a local gauge transformation which in this case takes form

$$\psi' = e^{i\Lambda(x)}\psi; \quad \bar{\psi}' = e^{-i\Lambda(x)}\bar{\psi} \tag{1.15}$$

When transforming (1.12) we obtain

$$\begin{aligned} \mathscr{L}_0' &= i\bar{\psi}'\gamma^\mu\partial_\mu\psi' - m\bar{\psi}'\psi' = ie^{-i\Lambda}\bar{\psi}\gamma^\mu(ie^{i\Lambda}\psi\partial_\mu\Lambda + e^{i\Lambda}\partial_\mu\psi) - m\bar{\psi}\psi \\ &= -\bar{\psi}\gamma^\mu\psi\partial_\mu\Lambda + i\bar{\psi}\gamma^\mu\partial_\mu\psi - m\bar{\psi}\psi = -\bar{\psi}\gamma^\mu\psi\partial_\mu\Lambda + \mathscr{L}_0 \end{aligned} \tag{1.16}$$

Therefore $\mathscr{L}_0$ is not invariant under local gauge transformation. Let us now try to cancel the term proportional to $\partial_\mu\Lambda$ by adding an interaction term involving a new vector field A_μ (called gauge field) whose transformation will cancel the non-invariant term in $\mathscr{L}_0'$. The interaction term will be

$$\mathscr{L}_{int} = g\bar{\psi}\gamma^\mu\psi A_\mu$$

where g is a coupling constant. The transformation of a vector field A_μ is required to be

$$A_\mu' = A_\mu + \frac{1}{g}\partial_\mu\Lambda \tag{1.17}$$

In case $\Lambda = g\chi$ we obtain a gauge transformation of the electromagnetic 4-potential. The extended Lagrangian

$$\mathscr{L} = \mathscr{L}_0 + \mathscr{L}_{int} \tag{1.18}$$

now transforms like

$$\begin{aligned} \mathscr{L}' &= \mathscr{L}_0' + g\bar{\psi}'\gamma^\mu\psi' A_\mu' = \mathscr{L}_0 - \bar{\psi}\gamma^\mu\psi\partial_\mu\Lambda + g\bar{\psi}\gamma^\mu\psi(A_\mu + \frac{1}{g}\partial_\mu\Lambda) \\ &= \mathscr{L}_0 + \mathscr{L}_{int} = \mathscr{L} \end{aligned} \tag{1.19}$$

It is common to write (1.18) as

$$\mathscr{L} = i\bar{\psi}\gamma^\mu(\partial_\mu - igA_\mu)\psi - m\bar{\psi}\psi = i\bar{\psi}\gamma^\mu D_\mu\psi - m\bar{\psi}\psi \tag{1.20}$$

where D_μ denotes covariant derivative, i.e. differential operator which transforms covariantly under gauge transformations (1.15) and (1.17), i.e. like ψ itself. In particular

$$D'_\mu = e^{i\Lambda} D_\mu e^{-i\Lambda}$$

This, together with (1.20), makes gauge invariance of the Lagrangian really transparent.

In order to get nontrivial Euler-Lagrange equations of motion for the A_μ we should add another term involving derivatives of A_μ (so called kinetic term). If we want to maintain gauge invariance of (1.20), this new term has to be also gauge invariant. Electromagnetic field tensor (1.11) fulfills these requirements. Finally we get

$$\mathscr{L}_{total} = -\frac{1}{4} F_{\mu\nu} F^{\mu\nu} + i\bar{\psi} \not{D} \psi - m\bar{\psi}\psi$$

where the coefficient of the kinetic term has been fixed to reproduce correctly Maxwell equations. Feynman slash $\not{D}$ is a common notation for $\gamma^\mu D_\mu$. It is worth noting, that the gauge field tensor $F_{\mu\nu}$ can be also obtained from commutator

$$-igF_{\mu\nu} = [D_\mu, D_\nu] \tag{1.21}$$

To sum up, starting with the requirement of a local gauge symmetry of a free matter-field Lagrangian we were forced to introduce an interaction involving a vector field (with specific transformation properties) and finally we got a Lagrangian of a Maxwell electromagnetic theory. It was a simple example of an successful heuristic principle which led to the formulation of a present-day Standard Model of particle physics.

1.4 Non-Abelian gauge theories

In the previous section, the gauge transformations formed group $U(1)$ which is Abelian, i.e. commutative. Natural question which now arises is whether it is possible to generalize the results of the preceding section to the field theory models involving a non-Abelian internal symmetry (e.g. isospin). It is indeed so as we will show on the example of Yang-Mills field (in the honour of C. N. Yang and R. Mills). Let us consider again a free-field Lagrangian

$$\mathscr{L}_0 = i\bar{\Psi}\gamma^\mu \partial_\mu \Psi - m\bar{\Psi}\Psi \tag{1.22}$$

where Ψ is a doublet of Dirac spinors (i.e. it has 8 components).

$$\Psi = \begin{pmatrix} \psi_1 \\ \psi_2 \end{pmatrix}$$

Similarly to the previous case, Lagrangian is invariant under global unitary transformation

$$\Psi' = U\Psi; \quad \bar{\Psi}' = \bar{\Psi}U^\dagger \tag{1.23}$$

where U is constant 2×2 unitary matrix. Nevertheless, we can restrict ourselves only to the matrices with unit determinant - $SU(2)$ group (these form the simplest suitable non-Abelian group). We will not lose anything because $U(2) = U(1) \otimes SU(2)$, and the $U(1)$ part can be treated in the already described way.

Any $SU(2)$ matrix S can be written in a form

$$S = \exp(i\Lambda^i T^i) \tag{1.24}$$

generators T^i defined as $T^i = \sigma^i/2$, where σ^i denote, as usual, Pauli matrices, and Λ^i are some complex parameters. Notation (1.24) is possible because $SU(2)$ is a Lie group. Its generators T^i forms corresponding Lie algebra with commutation relations

$$\left[T^i, T^j\right] = if^{ijk}T^k \tag{1.25}$$

where f^{ijk} denotes structure constants. In this case $f^{ijk} = \varepsilon^{ijk}$.

The (1.22) is again not invariant under local gauge transformations (i.e. when $\Lambda^i = \Lambda^i(x^\mu)$). Thus we will introduce a triplet of vector fields A^i_μ which together will form matrix

$$A_\mu(x^\mu) = A^i_\mu(x^\mu)T^i$$

Now we can formally define covariant derivative in a same way as in the Abelian case

$$\mathscr{L} = i\bar{\Psi}\gamma^\mu D_\mu\Psi - m\bar{\Psi}\Psi = i\bar{\Psi}\gamma^\mu(\partial_\mu - igA_\mu)\Psi - m\bar{\Psi}\Psi \tag{1.26}$$

Because we require D_μ to transform like

$$D'_\mu = SD_\mu S^\dagger = SD_\mu S^{-1}$$

where $D'_\mu = \partial_\mu - igA'_\mu$, matrix field A_μ must transform as follows

$$A'_\mu = SA_\mu S^{-1} + \frac{i}{g}S\partial_\mu S^{-1} \tag{1.27}$$

It can be easily proved ([1], chapter 4) that transformed field can be also decomposed to the triplet of components $A'_\mu = A^{i\prime}_\mu T^i$.

Although we have transformation law for the matrix field, it is generally not possible to write transformation relations for its components. The notable exception are infinitesimal gauge transformation. In this case the transformation matrix S can be used in form

$$S(x^\mu) = 1 + i\lambda^i(x^\mu)T^i; \quad S^{-1}(x^\mu) = 1 - i\lambda^i(x^\mu)T^i \tag{1.28}$$

where λ^i is an infinitesimal local parameter. Substituting (1.28) into (1.27), neglecting terms of $O(\lambda^2)$ and remembering relation (1.25) we will get

$$A^{i\prime}_\mu = A^i_\mu - f^{ijk}\lambda^j A^k_\mu + \frac{1}{g}\partial_\mu \lambda^i \tag{1.29}$$

In the case of $U(1)$ group all generators commute, so that the middle term in (1.29) vanishes and we get the known transformation of the electromagnetic potential (1.17).

The last step is the construction of the kinetic term. We can take inspiration from (1.21), so that

$$F_{\mu\nu} = \frac{i}{g}[D_\mu, D_\nu] \tag{1.30}$$

After some algebra one gets

$$F_{\mu\nu} = \partial_\mu A_\nu - \partial_\nu A_\mu - ig\,[A_\mu, A_\nu]$$

If we define components of a field tensor in the same way as for the interaction field (i.e. $F_{\mu\nu} = F^i_{\mu\nu}T^i$) we get

$$F^i_{\mu\nu} = \partial_\mu A^i_\nu - \partial_\nu A^i_\mu + g f^{ijk} A^j_\mu A^k_\nu$$

From definition (1.30) it is obvious that $F_{\mu\nu}$ transforms covariantly. For infinitesimal transformations of components it means that

$$F^{i\prime}_{\mu\nu} = F^i_{\mu\nu} - f^{ijk}\lambda^j F^k_{\mu\nu}$$

thus $F_{\mu\nu}$ is not gauge invariant. It can, nevertheless, be used to construct a quadratic invariant

$$\mathscr{L}_{kinetic} = c\mathrm{Tr}(F_{\mu\nu}F^{\mu\nu}) = \frac{1}{2}cF^i_{\mu\nu}F^{i\mu\nu}$$

where c is an arbitrary constant. The last equality is valid because

$$\mathrm{Tr}(T^i T^j) = \frac{1}{2}\delta^{ij}$$

If we set $c = -1/2$ for the best resemblance to the Abelian case, the final Lagrangian looks like

$$\mathscr{L}_{YM} = -\frac{1}{4}F^i_{\mu\nu}F^{i\mu\nu} + i\bar{\Psi}\not{D}\Psi - m\bar{\Psi}\Psi \tag{1.31}$$

The most interesting change, which has no analogy in Maxwell electrodynamics, is that the first term in (1.31) contains (in addition to expected kinetic terms) also cubic and quartic terms corresponding to self-interaction of the Yang-Mills fields.

From this general scheme we can construct gauge fields also for higher dimension groups (most common example is $SU(3)$ used in QCD) using the respective generators and structure constants. On the other hand, this way we can describe only massless gauge fields (as photon or gluons) but it fails to describe phenomenology of weak interactions. In the next section it will be briefly explained how to simultaneously introduce mass term and maintain gauge invariance.

1.5 Electroweak Interaction

1.5.1 Basic Ideas

The formulation of the standard model of electroweak interaction by S. L. Glashow, S. Weinberg and A. Salam (GWS) in the late 1960s was one of the most astonishing achievements of the 20th century physics. It has not only given one theoretical framework for rather different physical phenomena like parity-conserving long range electromagnetism and parity-violating short range weak interaction, but it has also (successfully) predicted the masses of intermediating bosons W. Moreover it predicted the existence of neutral intermediating boson Z which had been totally unexpected at that time (in the contrary to W bosons which were supposed to mediate interactions of charged and neutral leptons, e.g. β-decay). Another predicted phenomenon that was not previously expected was neutral current, i.e. interactions of the particles carrying the same charge mediated by Z boson.

The neutral weak current was indeed observed in 1970s in CERN and the bosons W and Z were discovered in 1983, also in CERN. As of 2006 the only unobserved prediction of GWS model is that of Higgs particle which should give masses to the intermediating bosons as well as to the other weakly interacting particles.

The appropriate group for electroweak unification is $SU(2) \times U(1)$. To incorporate different behaviour of electromagnetic and weak interaction, it is good to request different transformation properties from right-handed and left-handed components of lepton fields (1.13). It is convenient to introduce operator of chirality as 4×4 matrix

$$\gamma^5 = \begin{pmatrix} 1 & 0 \\ 0 & -1 \end{pmatrix} \tag{1.32}$$

Now we can define left-handed components of neutrino and electron as $\nu_L = 1/2(1-\gamma^5)\nu$ and $e_L = 1/2(1-\gamma^5)e$. Similarly $\nu_R = 1/2(1+\gamma^5)\nu$ and $e_R = 1/2(1+\gamma^5)e$. To describe proper phenomenology the electroweak theory we now require that left-handed components form $SU(2)$ doublet

$$L = \begin{pmatrix} \nu_L \\ e_L \end{pmatrix} \tag{1.33}$$

while right-handed components form $SU(2)$ singlets. Let us define the transformation properties of lepton and gauge fields under the subgroup $U(1)$ similarly as in the section 1.2.:

$$B'_\mu = B_\mu + \frac{1}{g}\partial_\mu \Lambda \tag{1.34}$$

$$\Psi' = e^{iY\Lambda}\Psi \tag{1.35}$$

B_μ denotes the Abelian gauge field, Ψ is a symbol of either singlet or doublet of fields and Y is a real parameter meaning that there are infinitely many representations of $U(1)$ group. To maintain invariance, covariant derivative takes form

$$D_\mu = \partial_\mu - igYB_\mu$$

We have introduced symmetry, so one can now ask, which properties are conserved. The $SU(2)$ symmetry stands for conservation of weak isospin, while $U(1)$ stands for weak hypercharge. Using experience from previous section we can now write down $SU(2) \times U(1)$ gauge invariant Lagrangian involving lepton interactions

$$\begin{aligned} \mathscr{L}_{lepton} = {} & i\bar{L}\gamma^\mu(\partial_\mu - igA^i_\mu \frac{\sigma^i}{2} - ig'Y_L B_\mu)L + i\bar{e}_R\gamma^\mu(\partial_\mu - ig'Y_R^{(e)}B_\mu)e_R + \\ & + i\bar{\nu}_R\gamma^\mu(\partial_\mu - ig'Y_R^{(\nu)}B_\mu)\nu_R \end{aligned} \tag{1.36}$$

where A^i_μ is the triplet of Yang-Mills gauge fields (from $SU(2)$ symmetry subgroup). In terms containing $SU(2)$ singlets the non-Abelian gauge fields are missing, because

the generators of group are trivial in this representation. Parameter Y represents (in all forms) weak hypercharge and its values are fixed by

$$Q = T_3 + Y$$

where Q is electric charge and T_3 is the third component of the weak isospin which behaves similarly like the strong isospin defined in the section 1.1. In particular, doublet members have the magnitude of spin 1/2 (T_3 then has values $\pm 1/2$), singlets have isospin of 0. So the hypercharge values

$$Y_L = -\frac{1}{2}, \qquad Y_R^{(e)} = -1 \qquad \text{and} \qquad Y_R^{(\nu)} = 0$$

denote also the average charge of a given multiplet. Notice that we have introduced two coupling constants, as our symmetry group can be decomposed to the product of two independent groups.

The gauge fields A_μ^i and B_μ need not have any direct physical meaning. Indeed, the physical vector fields are their linear combination. Let us consider the interaction part of (1.36)

$$\mathscr{L}_{lepton}^{(int)} = g\bar{L}\gamma^\mu \frac{\sigma^i}{2} L A_\mu^i + g' Y_L \bar{L}\gamma^\mu L B_\mu + g' Y_R^{(e)} \bar{e}_R \gamma^\mu e_R B_\mu + g' Y_R^{(\nu)} \bar{\nu}_R \gamma^\mu \nu_R B_\mu$$

This we could rewrite in a following form

$$\begin{aligned} \mathscr{L}_{lepton}^{(int)} &= g(\bar{L}\gamma^\mu \frac{\sigma^+}{2} L W_\mu^+ + \bar{L}\gamma^\mu \frac{\sigma^-}{2} L W_\mu^- + \bar{L}\gamma^\mu \frac{\sigma^3}{2} L A_\mu^3) + \dots \\ &= \frac{g}{\sqrt{2}}(\bar{\nu}_L \gamma^\mu e_L W_\mu^+ + \bar{e}_L \gamma^\mu \nu_L W_\mu^-) + \mathscr{L}_{diag} \end{aligned} \tag{1.37}$$

where $\sigma^\pm = 1/\sqrt{2}(\sigma^1 \pm i\sigma^2)$ and $W_\mu^\pm = 1/\sqrt{2}(A_\mu^1 \mp i A_\mu^2)$. $\mathscr{L}_{diag}$ denotes all remaining terms - these involving diagonal matrix (σ^3 or unit matrix). The first two terms in (1.37) contain the weak charged current (that is an interaction when participating particles exchange a W boson) and $W_\mu^\pm$ represents the couple of the intermediating bosons.

Lagrangian (1.36) should also describe electromagnetic interaction. When we work out the matrix multiplication in diagonal terms we get

$$\begin{aligned} \mathscr{L}_{diag} &= \frac{1}{2} g \bar{\nu}_L \gamma^\mu \nu_L A_\mu^3 - \frac{1}{2} g \bar{e}_L \gamma^\mu e_L A_\mu^3 + g' Y_L \bar{\nu}_L \gamma^\mu \nu_L B_\mu + g' Y_L \bar{e}_L \gamma^\mu e_L B_\mu + \\ &\quad + g' Y_R^{(\nu)} \bar{\nu}_R \gamma^\mu \nu_R B_\mu + g' Y_R^{(e)} \bar{e}_R \gamma^\mu e_R B_\mu \end{aligned}$$

It is now obvious that none of the fields A^3_μ and B_μ can be directly associated with electromagnetic field. They are coupled to the neutrino and there is no choice of (generally arbitrary) Y_L and Y_R that could make interaction fields coupled to electron only. This problem is solved when one considers an orthogonal transformation

$$\begin{aligned} A^3_\mu &= \cos\theta_W Z_\mu + \sin\theta_W A_\mu \\ B_\mu &= -\sin\theta_W Z_\mu + \cos\theta_W A_\mu \end{aligned} \tag{1.38}$$

where A_μ will be electromagnetic field and Z_μ will represent the new neutral vector field. The parameter of transformation θ_W is called the Weinberg angle or weak mixing angle. If we now write down the part of Lagrangian containing A_μ we get

$$\begin{aligned} \mathscr{L}^{(A)}_{diag} = \Big[&\frac{1}{2} g \bar{\nu}_L \gamma^\mu \nu_L \sin\theta_W - \frac{1}{2} g \bar{e}_L \gamma^\mu e_L \sin\theta_W + g' Y_L \bar{\nu}_L \gamma^\mu \nu_L \cos\theta_W + \\ &+ g' Y_L \bar{e}_L \gamma^\mu e_L \cos\theta_W + g' Y^{(\nu)}_R \bar{\nu}_R \gamma^\mu \nu_R \cos\theta_W + g' Y^{(e)}_R \bar{e}_R \gamma^\mu e_R \cos\theta_W \Big] A_\mu \end{aligned}$$

When we now require that the interaction does not involve neutrino and that it interacts with right-handed and left-handed component with equal strength (the interaction conserves parity), we will get three conditions:

$$Y^{(\nu)}_R = 0 \tag{1.39}$$

$$\frac{1}{2} g \sin\theta_W + Y_L g' \cos\theta_W = 0 \tag{1.40}$$

$$-\frac{1}{2} g \sin\theta_W + Y_L g' \cos\theta_W = Y^{(e)}_R g' \cos\theta_W \tag{1.41}$$

They are satisfied when

$$Y^{(e)}_R = 2Y_L \quad \text{and} \quad \tan\theta_W = -2Y_L \frac{g'}{g} \tag{1.42}$$

When we choose the conventional value of lepton hypercharge (i.e. $-1/2$) we will get following relations for weak mixing angle which links together coupling constants from both interactions

$$\cos\theta_W = \frac{g}{\sqrt{g^2 + g'^2}}\,, \quad \sin\theta_W = \frac{g'}{\sqrt{g^2 + g'^2}} \tag{1.43}$$

Because electromagnetic Lagrangian is conventionally written as

$$\mathscr{L}_{EM} = -e\ \bar{e}\gamma^\mu e A_\mu$$

we can obtain (from (1.41) and (1.42)) a relation between "classical" coupling constant e and gauge coupling

$$e = g \sin \theta_W \tag{1.44}$$

The term in $\mathscr{L}_{diag}$ containing neutral boson field Z_μ describes weak neutral currents. Using the relation (1.42) it can be recast as

$$\mathscr{L}^{(Z)}_{diag} = \frac{g}{\cos \theta_W} \left[\frac{1}{2} \bar{\nu}_L \gamma^\mu \nu_L + (\sin^2 \theta_W - \frac{1}{2}) \bar{e}_L \gamma^\mu e_L + \sin^2 \theta_W \bar{e}_R \gamma^\mu e_R \right] Z_\mu$$

Thus we have analyzed the $\mathscr{L}_{lepton}$. Now we should add appropriate kinetic term which is (in the spirit of the Yang-Mills construction)

$$\mathscr{L}_{gauge} = -\frac{1}{4} F^i_{\mu\nu} F^{i\mu\nu} - \frac{1}{4} B_{\mu\nu} B^{\mu\nu} \tag{1.45}$$

where,

$$F^i_{\mu\nu} = \partial_\mu A^i_\nu - \partial_\nu A^i_\mu + g \varepsilon^{ijk} A^j_\mu A^k_\nu \quad \text{and} \quad B_{\mu\nu} = \partial_\mu B_\nu - \partial_\nu B_\mu \tag{1.46}$$

1.5.2 Goldstone model

The Lagrangian $\mathscr{L}_{lepton} + \mathscr{L}_{gauge}$ constructed in the preceding section does not correctly describe what we can see in the experiment. Indeed (1.36) does not contain any mass term (i.e. term in the form $-m^2 \bar{\psi} \psi$ where m is an arbitrary positive constant), while we know from that both leptons and weak intermediating bosons have mass. It is also obvious that introducing such a terms in a straightforward way would break desired gauge symmetry of our Lagrangian. The way how to do this without destroying the symmetry is called Higgs mechanism (after P. Higgs). Its basic ingredient is the Goldstone phenomenon which is also the subject of this section.

Let us have a Lagrangian of a classical complex scalar field in the form

$$\mathscr{L} = \partial_\mu \phi \partial^\mu \phi^* + \mu^2 \phi \phi^* - \lambda (\phi \phi^*)^2 \tag{1.47}$$

where μ is a real parameter with the dimension of mass (note that it has "wrong sign") and λ is dimensionless positive coupling constant. Setting $\lambda = 0$ we will get Lagrangian that ultimately leads to the Klein-Gordon equation with reversed sign of mass squared.

Corresponding energy density is

$$\mathscr{H} = \partial_\mu \phi \partial^\mu \phi^* + \overbrace{(-\mu^2 \phi\phi^* + \lambda(\phi\phi^*)^2)}^{V(\phi)}$$

Let us find the state with the minimal energy. Contributions from derivative terms is always positive, so we should consider a constant field ϕ_0 and try to find a minimum of the "potential" $V(\phi)$. It is obvious that the "potential" is a function of one real variable $\rho^2 = \phi\phi^*$. Remembering that $\lambda > 0$ we easily find that the minimum of V corresponds $\rho = \pm\mu/\sqrt{2\lambda}$. Returning to the original variable ϕ we obtain a continuous one-parameter set of constant fields

$$\phi_0 = \frac{v}{\sqrt{2}} e^{i\alpha} \tag{1.48}$$

where $v = \mu/\sqrt{\lambda}$ and α is an arbitrary real parameter. The ground state is thus infinitely degenerate. The existence of a non-zero ground state led J. Goldstone to the idea that it would be more reasonable to study small oscillations around this ground state rather than using $\phi = 0$ as a reference point.

The first step is to factorize the field in a way

$$\phi(x) = \rho(x) \exp\left(i\frac{\pi(x)}{v}\right) \tag{1.49}$$

and rewrite the "potential" as

$$V(\rho) = -\mu^2\rho^2 + \lambda\rho^4 = \lambda\left[\left(\rho^2 - \frac{\mu^2}{2\lambda}\right)^2 - \left(\frac{\mu^2}{2\lambda}\right)^2\right] = \lambda\left(\rho^2 - \frac{\mu^2}{2\lambda}\right)^2 - \frac{1}{4}\lambda v^4 \tag{1.50}$$

where ρ and π are radial and angular field variables. The factor $1/v$ in (1.49) guarantees that π has the right dimension of mass. Because without losing anything essential we can drop the additive constant from (1.50), the Lagrangian (1.47) can be written in a form

$$\mathscr{L} = \partial_\mu \rho \partial^\mu \rho + \frac{1}{v^2}\rho^2 \partial_\mu \pi \partial^\mu \pi - \lambda\left(\rho^2 - \frac{\mu^2}{2\lambda}\right)^2 \tag{1.51}$$

Now its time to do what was suggested above. Let us introduce new field variable σ by relation

$$\rho = \frac{1}{\sqrt{2}}(\sigma + v) \tag{1.52}$$

The factor $1/\sqrt{2}$ was chosen to get proper normalization. Substituting (1.52) into (1.51) one gets

$$\mathscr{L} = \frac{1}{2}\partial_\mu\sigma\partial^\mu\sigma + \frac{1}{2}\partial_\mu\pi\partial^\mu\pi - \lambda v^2\sigma^2 + \text{interaction terms} \tag{1.53}$$

where we denoted all terms higher than quadratic in fields or their derivatives as "interaction terms". The result of all this is that instead of a complex field ϕ with wrong mass sign we now have two real fields σ and π. One is massless (π) while the other has mass with right sign, i.e. $1/2\ m_\sigma^2 = \lambda v^2$.

To sum up, we started with Lagrangian which was invariant under transformation $\phi' = e^{i\alpha}\phi$. However, its ground state lost this symmetry, so the situation which is usually called "spontaneous symmetry breaking" occurred. This made us realize that (1.47) describes in fact one massive scalar field σ and one massless field π, which corresponds to the so-called Goldstone boson. If we rewrite transformation law in terms of this new variables we get

$$\sigma' = \sigma, \quad \pi' = \pi + v\alpha$$

so we did not lose the Lagrangian invariance. This observation can be generalized by Goldstone theorem which says that if a global continuous symmetry is spontaneously broken, then there exist one massless scalar particle for each broken generator of the original symmetry. Proof of this statement can be found in [4].

1.5.3 Higgs Mechanism for $SU(2) \otimes U(1)$ gauge symmetry

Now we would like to introduce 3 massive vector bosons which we observe during experiments. So we will need 3 Goldstone bosons. But because at least one scalar boson survives the Higgs mechanism, we will need at least 4 real scalar fields. Let us construct a (doublet) representation of $SU(2)$ group as

$$\Phi = \begin{pmatrix} \phi^+ \\ \phi^0 \end{pmatrix} = \begin{pmatrix} \phi_1 + i\phi_2 \\ \phi_3 + i\phi_4 \end{pmatrix}$$

where ϕ^+ and ϕ^0 are complex and ϕ_j are real.

Our key purpose when constructing Lagrangian is that it remains gauge invariant. In analogy with previous section (in particular with (1.47)) we should introduce Lagrangian that is $SU(2)$ invariant:

$$\mathscr{L} = (\partial_\mu\Phi^\dagger)(\partial^\mu\Phi)\overbrace{+\mu^2\Phi^\dagger\Phi - \lambda(\Phi^\dagger\Phi)^2}^{-V(\Phi)}$$

Similarly to the preceding section we can find that "potential" V is minimal for

$$\Phi_0^\dagger \Phi_0 = \frac{v^2}{2}; \quad v = \frac{\mu}{\sqrt{\lambda}}$$

When we shift the ground state value to the level of minimal energy, we obtain

$$\mathscr{L} = (\partial_\mu \Phi^\dagger)(\partial^\mu \Phi) - \lambda(\Phi^\dagger \Phi - \frac{v^2}{2})^2 \tag{1.54}$$

Now we have to make (1.54) locally $SU(2) \otimes U(1)$ invariant. The Φ itself is not only $SU(2)$ doublet, but also carries weak hypercharge Y associated with $U(1)$. Because the "potential" part of Lagrangian has already the required symmetry, it will be sufficient to change normal derivatives to covariant as we have done in previous sections. Resulting Lagrangian is then

$$\mathscr{L}_{Higgs} = \Phi^\dagger (\overleftarrow{\partial_\mu} + igA_\mu^j \frac{\sigma^j}{2} + ig' Y B_\mu)(\overrightarrow{\partial^\mu} - igA^{k\mu}\frac{\sigma^k}{2} - ig' Y B^\mu)\Phi - \lambda(\Phi^\dagger \Phi - \frac{v^2}{2})^2 \tag{1.55}$$

where the arrows denote in which direction the derivatives act, A_μ^j and B_μ are Yang-Mills gauge fields which were introduced to maintain local gauge symmetry (in the same way as in the sections 1.4 or 1.5.1), σ^j are Pauli matrices and g, g' are coupling constants of respective fields.

Continuing in analogy with the previous section (cf. (1.49)) , we should factorize Φ. This can be done as

$$\Phi(x) = \exp\left(\frac{i}{v}\pi^j(x)\sigma^j\right)\begin{pmatrix} 0 \\ \frac{1}{\sqrt{2}}(v + H(x)) \end{pmatrix} \tag{1.56}$$

where we have already done the shift of radial variable (ρ in (1.49)) and π^j are Goldstone bosons.

The transformation which we use is unitary, i.e. it does not change the norm of Φ. However, it can change its "phase". In particular it means, that there is a gauge transformation for which

$$\exp\left(\frac{i}{v}\pi^j(x)\sigma^j\right) \to \mathbf{1} \quad \text{i.e.} \quad \pi^j \to 0 \tag{1.57}$$

This is called U-gauge. Of course, the transformation affects also gauge fields, but, as their transformation properties were mentioned earlier (1.27 and 1.17) we shall not write them explicitly this time. Complex doublet Φ now transforms like

$$\Phi(x) \to \Phi_U(x) = \begin{pmatrix} 0 \\ \frac{1}{\sqrt{2}}(v + H(x)) \end{pmatrix} \tag{1.58}$$

We shall remember, that this transformation changes also gauge fields A^j_μ and B_μ, but for the sake of simplicity, we will denote the transformed fields in the same way as the old ones (anyway, there was nothing special about the original fields). When we write Φ_U as

$$\Psi_U(x) = \frac{1}{\sqrt{2}}(v + H(x))\xi, \quad \text{where} \quad \xi = \begin{pmatrix} 0 \\ 1 \end{pmatrix} \tag{1.59}$$

and use the well known relations for Pauli matrices

$$\sigma^i\sigma^j + \sigma^j\sigma^i = 2\delta^{ij}\mathbf{1} \tag{1.60}$$

$$\xi^\dagger\sigma^i\xi = -\delta^{3i} \tag{1.61}$$

$$\xi^\dagger\xi = 1 \tag{1.62}$$

one can get, after some algebra

$$\begin{aligned} \mathscr{L}^{(U)}_{Higgs} &= \frac{1}{2}\partial_\mu H \partial^\mu H - \lambda v^2 H^2 - \lambda v H^3 - \frac{1}{4}\lambda H^4 + \\ &+ \frac{1}{8}(v+H)^2(g^2 A^j_\mu A^{j\mu} - 4Y g g' A^3_\mu B^\mu + 4Y^2 g'^2 B_\mu B^\mu) \end{aligned} \tag{1.63}$$

Focusing on the relevant mass term (i.e. quadratic in fields) we get

$$\mathscr{L}_{mass} = \frac{1}{8}v^2\left[g^2\left(\left(A^1_\mu\right)^2 + \left(A^2_\mu\right)^2\right) + \left(gA^3_\mu - 2g'YB_\mu\right)^2\right] \tag{1.64}$$

This we now adjust to such a form where we will see familiar terms for vector bosons known from previous section

$$\begin{aligned} \mathscr{L}_{mass} &= \frac{1}{8}\left(g^2 + 4g'^2Y^2\right)v^2\left(\frac{g}{\sqrt{g^2+4g'^2Y^2}}A^3_\mu - \frac{2Yg'}{\sqrt{g^2+4g'^2Y^2}}B_\mu\right)^2 + \\ &+ \frac{1}{4}g^2v^2W^-_\mu W^{+\mu} \end{aligned} \tag{1.65}$$

where we used $W^\pm_\mu = 1/\sqrt{2}(A^1_\mu \mp iA^2_\mu)$ (cf. 1.37). We can also find the neutral boson Z_μ in the above relation. Writing inverse transformation to (1.38) we find that

$$Z_\mu = \cos\theta_W A^3_\mu - \sin\theta_W B_\mu \tag{1.66}$$

Using the relations (1.43) it is easy to see that when we set the Higgs boson weak hypercharge $Y = 1/2$ we get the mass term for boson Z_μ. To be exhaustive, we can introduce a gauge field A_μ (electromagnetic field) which is orthogonal to Z_μ, i.e. the same situation as in section 1.4.

$$A_\mu = \frac{1}{\sqrt{g^2 + g'^2}}(g' A_\mu^3 + g B_\mu) \tag{1.67}$$

where we had already put the conventional value of hypercharge Y. This field is massless, because there is no such term in (1.65).

To sum up, we started with three Goldstone bosons (they emerged from spontaneously broken $SU(2)$ symmetry), which were, however, unphysical - gauge transformation made them disappear. On the other hand we got three massive bosons $W^\pm$ and Z as well as massive Higgs boson. Their masses can be easily obtained from (1.65), (1.66 and (1.63)

$$m_W = \frac{1}{2} g v \tag{1.68}$$

$$m_Z = \frac{1}{2}\sqrt{g^2 + g'^2}\, v \tag{1.69}$$

$$m_H = \sqrt{2\lambda}\, v \tag{1.70}$$

To see which parameters are free (i.e. their value comes from the experiment, not from the theory itself) it is worth to rewrite boson masses as well as vacuum value of the Higgs field in following way

$$\begin{aligned} m_W &= \left(\frac{\pi\alpha}{G_F\sqrt{2}}\right)^{\frac{1}{2}} \frac{1}{\sin\theta_W} \\ m_Z &= \left(\frac{\pi\alpha}{G_F\sqrt{2}}\right)^{\frac{1}{2}} \frac{1}{\sin\theta_W \cos\theta_W} \\ v &= \frac{1}{(G_F\sqrt{2})^{\frac{1}{2}}} \end{aligned} \tag{1.71}$$

where we use the Fermi constant G_F, fine structure constant α and unification condition for electromagnetic coupling constant:

$$\frac{G_F}{\sqrt{2}} = \frac{g^2}{8m_W^2}, \quad \alpha = \frac{e^2}{4\pi}, \quad e = g\sin\theta_W \tag{1.72}$$

From (1.71) and (1.63) we see that the masses of $W^{\pm}$ and Z are subject to two independent parameters G_F and θ_W (which can be measured), while the mass of the Higgs boson is dependent on totally unknown parameter λ. We will close this section with the current[2] experimental values

$$\begin{aligned} m_W &= 80.425 \pm 0.038 \text{ GeV} \\ m_Z &= 91.1876 \pm 0.0021 \text{ GeV} \\ \sin^2\theta_W &= 0.23120 \pm 0.00015 \\ G_F &= 1.16637 \pm 0.00001 \times 10^{-5} \text{ GeV}^{-2} \end{aligned} \tag{1.73}$$

1.5.4 Lepton masses

Previous section showed how to add masses to the interaction bosons and maintain desired gauge invariance in the same time. However, we know that also leptons have masses, but the Lagrangian (1.36) does not have any mass terms. This can be fixed when we employ Yukawa-type coupling, which will be done in this section. Let us have a left-handed $SU(2)$ doublet

$$L = \begin{pmatrix} \nu_L \\ e_L \end{pmatrix} \tag{1.74}$$

the right-handed singlet e_R and the Higgs doublet Φ. From that we can build an $SU(2)$ invariant term

$$\mathscr{L}_{Yukawa} = -h_e \bar{L}\Phi e_R - h_e \overline{\bar{L}\Phi e_R} \tag{1.75}$$

One can see that (1.75) is also invariant under weak hypercharge $U(1)$: hypercharge of $\bar{L}$ is $Y_{\bar{L}} = -Y_L = 1/2$, $Y_\Phi = 1/2$ and $Y_R^{(e)} = -1$. Together we get $Y_{\bar{L}} + Y_\Phi + Y_R^{(e)} = 0$. Similarly to the previous section, we can now use unitary gauge transformation on (1.75):

$$\begin{aligned} \mathscr{L}^{(U)}_{Yukawa} &= -h_e(\bar{\nu}_L,\, \bar{e}_L) \begin{pmatrix} 0 \\ \frac{1}{\sqrt{2}}(v+H) \end{pmatrix} e_R - h_e \overline{\bar{\nu}_L,\, \bar{e}_L) \begin{pmatrix} 0 \\ \frac{1}{\sqrt{2}}(v+H) \end{pmatrix} e_R} \\ &= -\frac{1}{\sqrt{2}} h_e (v+H) \bar{e}_L e_R - \frac{1}{\sqrt{2}} h_e (v+H) \overline{\bar{e}_L e_R} \\ &= -\frac{1}{\sqrt{2}} h_e v \bar{e}e - \frac{1}{\sqrt{2}} h_e \bar{e}eH \end{aligned} \tag{1.76}$$

[2] data from 2002, cf. [5]

Here we can see an electron mass term

$$m_e = \frac{1}{\sqrt{2}} h_e v$$

The second term means interaction of the electron and the Higgs field. Its strength is determined by coupling constant

$$g_{eeH} = -\frac{1}{\sqrt{2}} h_e = -\frac{m_e}{v}$$

This approach can be of course simply generalized to the different charged lepton types like μ or τ.

Because recent experiments (e.g. Super-Kamiokande) have shown that neutrino mass is non-zero, natural question arises: Is it possible to give mass to the neutrino through the same mechanism that gives mass to the electron?

It is easy to realize that it is impossible to construct a $SU(2) \otimes U(1)$ invariant out of the doublets Φ and L and the singlet ν_R - the hypercharge assignments ($Y_R^\nu = 0$) would break the $U(1)$ invariance. However, we can use a trick. Let us define a new Higgs doublet as

$$\tilde{\Phi} = i \begin{pmatrix} 0 & -i \\ i & 0 \end{pmatrix} \Phi^* \tag{1.77}$$

where Φ^* is a complex conjugate to the original Higgs doublet Φ. We may also see that the transformation matrix in (1.77) is in fact the second Pauli matrix σ_2. It can be shown that this quantity transforms in the same way like Φ itself (cf. [1]). From the transforming properties under $U(1)$ (see (1.35)) one can see that complex conjugation changes the hypercharge sign. Thus, we have now $Y_{\tilde{\Phi}} = -1/2$. We can now construct the invariant

$$\widetilde{\mathscr{L}}_{Yukawa} = -h_\nu \bar{L} \tilde{\Phi} \nu_R - h_\nu \overline{\bar{L} \tilde{\Phi} \nu_R} \tag{1.78}$$

After applying the unitary gauge transformation and repeating the process from the previous paragraph we get

$$\widetilde{\mathscr{L}}^{(U)}_{Yukawa} = -\frac{1}{\sqrt{2}} h_\nu v \bar{\nu}\nu - \frac{1}{\sqrt{2}} h_\nu \bar{\nu}\nu H$$

Thus the neutrino mass and the Yukawa coupling constant are

$$m_\nu = \frac{1}{\sqrt{2}} h_\nu v \qquad \text{and} \qquad g_{\nu\nu H} = -\frac{m_\nu}{v}$$

1.5.5 The electroweak interaction of quarks

So far we were interested only in leptons. But, as was said earlier, the weak interaction affects also quarks. One can now ask if it is possible to incorporate lepton interaction into Lagrangian we have been constructing in the previous sections

$$\mathscr{L} = \mathscr{L}_{lepton} + \mathscr{L}_{gauge} + \mathscr{L}_{Higgs} + \mathscr{L}_{Yukawa} \tag{1.79}$$

whose parts were described above (cf. (1.36), (1.45), (1.55), (1.75)). Because $\mathscr{L}_{Higgs}$ and $\mathscr{L}_{gauge}$ do not contain any lepton fields, they will remain unchanged after the addition of quarks. Let us therefore focus on $\mathscr{L}_{lepton}$ and $\mathscr{L}_{Yukawa}$. The extension of the Lagrangian can be done quite easily and naturally. Let us have three $SU(2)$ doublets

$$L_0^{(d)} = \begin{pmatrix} u_{0L} \\ d_{0L} \end{pmatrix}, \quad L_0^{(s)} = \begin{pmatrix} c_{0L} \\ s_{0L} \end{pmatrix}, \quad L_0^{(b)} = \begin{pmatrix} t_{0L} \\ b_{0L} \end{pmatrix} \tag{1.80}$$

and six $SU(2)$ singlets u_{0R}, d_{0R}, c_{0R}, s_{0R}, t_{0R}, b_{0R}, where u, d, c, s, t, b stand for up, down, charm, etc. (cf. table 1.2) and indices L, R denote left-handed and right-handed components respectively.

Quarks doublets and singlets were constructed in analogy with lepton doublets (1.33) and singlets, so they could be used in a similar way. Indeed nothing prevents us from extending $\mathscr{L}_{lepton}$ (1.36) to

$$\begin{aligned}
\mathscr{L}_{fermion} &= \sum_{\ell=e,\mu,\tau} i\bar{L}^{(\ell)}\gamma^\mu(\partial_\mu - igA_\mu^j\frac{\sigma^j}{2} - iY_L^{(\ell)}g'B_\mu)L^{(\ell)} + \\
&+ \sum_{q=d,s,b} i\bar{L}_0^{(q)}\gamma^\mu(\partial_\mu - igA_\mu^j\frac{\sigma^j}{2} - iY_L^{(q)}g'B_\mu)L_0^{(q)} + \\
&+ \sum_{\ell=e,\mu,\tau,\nu^e,\nu^\mu,\nu^\tau} i\bar{\ell}_R\gamma^\mu(\partial_\mu - iY_R^{(\ell)}g'B_\mu)\ell_R + \\
&+ \sum_{q=d,u,s,c,b,t} i\bar{q}_{0R}\gamma^\mu(\partial_\mu - iY_R^{(q)}g'B_\mu)q_{0R}
\end{aligned} \tag{1.81}$$

where we introduced also the other two generations of leptons. The lepton doublets are defined as follows

$$L^{(e)} = \begin{pmatrix} \nu_{eL} \\ e_L \end{pmatrix}, \quad L^{(\mu)} = \begin{pmatrix} \nu_{\mu L} \\ \mu_L \end{pmatrix}, \quad L^{(\tau)} = \begin{pmatrix} \nu_{\tau L} \\ \tau_L \end{pmatrix} \tag{1.82}$$

The hypercharge assignment must obey the relation

$$Q = T_3 + Y$$

Using the values from the table 1.2 one gets

$$Y_L^{(\ell)} = -\frac{1}{2}\ (\ell = e, \mu, \tau), \quad Y_R^{(\ell)} = -1\ (\ell = e, \mu, \tau), \quad Y_R^{(\ell)} = 0\ (\ell = \nu_e, \nu_\mu, \nu_\tau)$$
$$Y_L^{(q)} = +\frac{1}{6}\ (q = d, s, b), \quad Y_R^{(q)} = -\frac{1}{3}\ (q = d, s, b), \quad Y_R^{(q)} = +\frac{2}{3}\ (q = u, c, t)$$

Lagrangian (1.81) was constructed in rather formal way treating the quarks like "leptons of other type". So we shall now ask if (1.81) has any physical meaning. We already know from the previous section that Yang-Mills fields A_μ^j and B_μ are only linear combination of physical fields. If we introduce $W_\mu^\pm$, Z_μ and A_μ in the same way as in the preceding sections, we can identify lepton charged currents as (cf. (1.37))

$$\mathscr{L}_{CC}^{(\ell)} = \frac{g}{2\sqrt{2}}\bar{\nu}_\ell\gamma^\mu(1-\gamma_5)\ell W_\mu^+ + \text{hermitian conjugate}$$

where γ_5 is an operator of chirality (see (1.32)). However the appropriate quark charged current Lagrangian would look like

$$\mathscr{L}_{CC}^{(u,d)} = \frac{g}{2\sqrt{2}}\bar{u_0}\gamma^\mu(1-\gamma_5)d_0 W_\mu^+ + \text{hermitian conjugate}$$

which is in strong disagreement with the Lagrangian, which was derived before GWS Standard Model and was generally accepted as correctly describing the quark charged current phenomenology

$$\mathscr{L}_{CC}^{(u,d,s)} = \frac{g}{2\sqrt{2}}\bar{u}\gamma^\mu(1-\gamma_5)(d\cos\theta_C + s\sin\theta_C)W_\mu^+ + \text{hermitian conjugate} \quad (1.83)$$

where θ_C denotes the Cabibbo angle. Thus we can conclude, that fields q_0, where q denotes the flavour of particular quark, do not have direct physical meaning, but they rather are (as in the case with the Yang-Mills fields) a linear combination of the physical quark fields.

To find relevant transformation, we will make a step aside. Apart from $\mathscr{L}_{lepton}$ the lepton fields could also be found in the $\mathscr{L}_{Yukawa}$. So let us formally extend the Yukawa part in the most general way (which holds $SU(2)\otimes U(1)$ invariance)

$$\mathscr{L}_{Yukawa}^{(q)} = -\sum_{\substack{q=d,s,b\\ q'=d,s,b}}\left(h_{qq'}\bar{L}_0^{(q)}\Phi q'_{0R} + \text{h.c.}\right) - \sum_{\substack{q=d,s,b\\ q'=u,c,t}}\left(\tilde{h}_{qq'}\bar{L}_0^{(q)}\tilde{\Phi}q'_{0R} + \text{h.c.}\right) \quad (1.84)$$

where Φ denotes Higgs scalar and $\tilde{\Phi}$ its "complex conjugate" (1.77). We wrote only the quark part (the lepton part has already been examined in the previous

section). From the construction it is obvious that Lagrangian remained $SU(2)\times U(1)$ invariant. Note that in this case $h_{qq'}$ and $\tilde{h}_{qq'}$ are generally complex. When we apply unitary gauge transformation on the (1.84) (defined in the same way as in the preceding sections) we will get

$$\begin{aligned}\mathscr{L}^{(q)}_{Yukawa} &= -\frac{1}{\sqrt{2}}(v+H)(\bar{d}_{0L},\bar{s}_{0L},\bar{b}_{0L})\begin{pmatrix} h_{dd} & h_{ds} & h_{db}\\ h_{sd} & h_{ss} & h_{sb}\\ h_{bd} & h_{bs} & h_{bb}\end{pmatrix}\begin{pmatrix} d_{0R}\\ s_{0R}\\ b_{0R}\end{pmatrix} + \text{h.c.}\\ &\quad -\frac{1}{\sqrt{2}}(v+H)(\bar{u}_{0L},\bar{c}_{0L},\bar{t}_{0L})\begin{pmatrix} \tilde{h}_{uu} & \tilde{h}_{uc} & \tilde{h}_{ut}\\ \tilde{h}_{cu} & \tilde{h}_{cc} & \tilde{h}_{ct}\\ \tilde{h}_{tu} & \tilde{h}_{tc} & \tilde{h}_{tt}\end{pmatrix}\begin{pmatrix} u_{0R}\\ c_{0R}\\ t_{0R}\end{pmatrix} + \text{h.c.}\end{aligned}$$

Working out the matrix multiplication we will get not only desired mass terms but also interaction terms. We will get rid of them using the fact, that every nonsingular square complex matrix M can be decomposed[3] as

$$M = \mathcal{U}^{\dagger}\mathfrak{M}\mathcal{V}$$

where $\mathcal{U}$ and$\mathcal{V}$ are unitary matrices and $\mathfrak{M}$ is diagonal and positive.

Both matrices $h_{qq'}$ and $\tilde{h}_{qq'}$ are nonsingular (otherwise we would get zero quark masses) so they could be diagonalized by means of biunitary transformation. Let us transform quark fields as

$$\begin{aligned}\begin{pmatrix} d_L\\ s_L\\ b_L\end{pmatrix} &= \mathcal{U}\begin{pmatrix} d_{0L}\\ s_{0L}\\ b_{0L}\end{pmatrix}, \quad \begin{pmatrix} d_R\\ s_R\\ b_R\end{pmatrix} = \mathcal{V}\begin{pmatrix} d_{0R}\\ s_{0R}\\ b_{0R}\end{pmatrix},\\ \begin{pmatrix} u_L\\ c_L\\ t_L\end{pmatrix} &= \tilde{\mathcal{U}}\begin{pmatrix} u_{0L}\\ c_{0L}\\ t_{0L}\end{pmatrix}, \quad \begin{pmatrix} u_R\\ c_R\\ t_R\end{pmatrix} = \tilde{\mathcal{V}}\begin{pmatrix} d_{0R}\\ s_{0R}\\ b_{0R}\end{pmatrix}\end{aligned} \tag{1.85}$$

It is clear that $\mathscr{L}^{(q)}_{Yukawa}$ now have only mass terms, so we have a good reason to identify the fields u, d, c, s, t, b with quarks.

Let us return to our original problem with the charged current. Substituting

[3]Proof of this statement could be found in [1], chapter 7.4

(1.85) into (1.81) we get the charged current term in form

$$\begin{aligned}\mathscr{L}_{CC}^{(quark)} &= \frac{g}{\sqrt{2}}(\bar{u}_{0L},\bar{c}_{0L},\bar{t}_{0L})\gamma^{\mu}\begin{pmatrix} d_{0L}\\ s_{0L}\\ b_{0L}\end{pmatrix}W_{\mu}^{+}+\text{h.c.}=\\ &= \frac{g}{\sqrt{2}}(\bar{u}_{L},\bar{c}_{L},\bar{t}_{L})\gamma^{\mu}\tilde{\mathcal{U}}\mathcal{U}^{\dagger}\begin{pmatrix} d_{L}\\ s_{L}\\ b_{L}\end{pmatrix}W_{\mu}^{+}+\text{h.c.}\end{aligned} \tag{1.86}$$

Matrix $V=\tilde{\mathcal{U}}\mathcal{U}^{\dagger}$ has nine complex (18 real) parameters. But $\mathcal{U}$ is unitary, so that also V is unitary which means, that V has 9 real parameters. However, we can go further. Without the loss of generality we can factor out the complex phase factors from the first column and put them into the front line vector of quark fields. We can do the same in the first row, remembering that the $[1,1]$ element is already real.

The essential part of (1.86) then become

$$(\bar{u}_{L}e^{i\delta_{11}},\bar{c}_{L}e^{i\delta_{21}},\bar{t}_{L}e^{i\delta_{31}})\begin{pmatrix} R_{11} & R_{12} & R_{13}\\ R_{21} & V_{22}e^{-i\delta_{21}}e^{-i\delta'_{12}} & V_{23}e^{-i\delta_{21}}e^{-i\delta'_{13}}\\ R_{31} & V_{32}e^{-i\delta_{31}}e^{-i\delta'_{12}} & V_{33}e^{-i\delta_{31}}e^{-i\delta'_{13}}\end{pmatrix}\begin{pmatrix} d_{L}\\ s_{L}e^{i\delta'_{12}}\\ b_{L}e^{i\delta'_{13}}\end{pmatrix} \tag{1.87}$$

which can be recast as

$$(\bar{u}'_{L},\bar{c}'_{L},\bar{t}'_{L})\begin{pmatrix} R_{11} & R_{12} & R_{13}\\ R_{21} & V''_{22} & V''_{23}\\ R_{31} & V''_{32} & V''_{33}\end{pmatrix}\begin{pmatrix} d_{L}\\ s'_{L}\\ b'_{L}\end{pmatrix} \tag{1.88}$$

because the change of the complex phase does not change the physical meaning of the field. We ignored the other parts of (1.86) because they act only as numerical factors. Thus we got rid of five complex phase factors and matrix V is now dependent on only four real parameters. Such a parametrization of V is called Cabibbo-Kobayashi-Maskawa matrix (or CKM matrix for short). If the V was purely real from the beginning (i.e. V would be an orthogonal matrix), it would be parameterized by three angles, therefore the fourth parameter is a complex phase.

Now it is time to ask if this process solved our original problem with the wrong Lagrangian for the quark charged current. Because (1.83) does not contain particles from the third generation of mass, we can restrict ourselves to two dimensions. General matrix V now have 4 real parameters, from which only one will remain after we factor out the complex phases from the first row and column. As a result

the two-dimensional CKM matrix now represents rotation in a plane. The charged current Lagrangian then becomes

$$\mathscr{L}_{CC}^{(quark)} = \frac{g}{\sqrt{2}}(\bar{u}_L, \bar{c}_L)\gamma^\mu \begin{pmatrix} \cos\theta_C & \sin\theta_C \\ -\sin\theta_C & \cos\theta_C \end{pmatrix} \begin{pmatrix} d_L \\ s_L \end{pmatrix} W_\mu^+ + \text{h.c.} \tag{1.89}$$

When we work out the matrix multiplication we will get the right charged current Lagrangian (1.83). Moreover, we will get also the term describing c, d, s quark charged current which is missing in the original theory, as quark c was not observed until 1970s.

The existence of nontrivial complex phase of CKM matrix has one notable consequence. The elements of CKM matrix determine (up to a real factor) the coupling constants of W bosons and quarks - so that these constants can be complex. We will see that under this condition the interaction Lagrangian is no longer $\mathcal{CP}$ invariant. Let us write down a part of (1.89) describing the interaction of quarks q_1 and q_2

$$\mathscr{L}_{int}^{(12)} = g_{12}\bar{q}_1\gamma^\mu(1-\gamma_5)q_2W_\mu^+ + g_{12}^*\bar{q}_2\gamma^\mu(1-\gamma_5)q_1W_\mu^- \tag{1.90}$$

After charge and parity conjugation, the Lagrangian looks like

$$\mathscr{L}_{int}^{(12)\prime} = g_{12}\bar{q}_2\gamma_\mu(1-\gamma_5)q_1W^{-\mu} + g_{12}^*\bar{q}_1\gamma_\mu(1-\gamma_5)q_2W^{+\mu} \tag{1.91}$$

thus for $g_{12}^* \neq g_{12}$ we have lost the universal $\mathcal{CP}$ invariance (which is a long known experimental fact). Note that three is the lowest number of fermion generations for which the theory allows $\mathcal{CP}$ violation.

Finally we will make a brief conclusion of this introduction to the GWS Standard Model. It is a gauge theory based on local $SU(2) \times U(1)$ symmetry and its Lagrangian can be written as

$$\mathscr{L} = \mathscr{L}_{fermion} + \mathscr{L}_{gauge} + \mathscr{L}_{Higgs} + \mathscr{L}_{Yukawa} \tag{1.92}$$

whose parts can be retrieved from (1.81), (1.45) and (1.55). Although we did not write complete $\mathscr{L}_{Yukawa}$ explicitly, it can be easily composed from (1.75), (1.78) and (1.84). However this mathematically elegant form does not have direct physical meaning - to achieve that we have to transform fields A_μ^j and B_μ to the fields $W_\mu^\pm$, Z_μ and A_μ, and the quark fields q_0 to the q.

Since its development in the late 1960s the GWS theory has met with tremendous phenomenological success: it predicted (among others) the existence and masses of intermediating bosons as well as the neutral weak current. All this phenomena were later observed and measured values confirmed the predictions of GWS Standard

Model. Nevertheless, it also predicted the existence of Higgs boson giving masses to the intermediating bosons and leptons, which has not been observed so far. This is one of the main reasons why the new collider is being built in CERN - if the Higgs particle exist, it should be found there.

The last remark concerns the number of free parameters inside GWS Standard Model. First of all, there ale coupling constants g, g', λ and "vacuum value" of Higgs field v. They could be expressed in terms of other physical constants (e.g. α, $\sin^2\theta_W$, m_Z and m_H), but there would be still four of them. Then there are particle masses: we have six lepton masses, six quark masses, four parameters of quark CKM matrix and four parameters of the lepton CKM matrix - that is 24 free parameters altogether. Such a high number suggests that Standard Model is not an ultimate theory of elementary particles, so the new discoveries at higher energies obtained from LHC could lead us to the more fundamental theory.

1.6 Quantum Chromodynamics

The last part of the Standard Model is the theory of the strong interaction. Similarly to the GWS electroweak theory, the QCD is also a non-Abelian gauge theory based in this case on a symmetry group $SU(3)$. Why this particular symmetry?

The Gell-Mann Eightfold Way brought order among hadrons, but created a new mystery: it was Δ^{++} resonance particle which has spin 3/2, but according to the Eightfold way it is composed from three u quarks which will therefore all have parallel spins, thus violating Pauli exclusion principle. This problem was solved by introducing another degree of freedom, later called colour charge. Because baryons are composed from three quarks and we perceive them as colour neutral, it was proposed that quarks can have "red", "green" or "blue" colour. This particular choice suggests that when this three quarks mix together, the resulting colour is "white", i.e. the baryons are colour neutral.

Antiquarks were assigned anticolours, so mesons (composed of quark-antiquark pair) are also colour neutral. And because it does not matter which particular quark in baryon is red, which green and which blue (as long as all colours are present), a $SU(3)$ symmetry was chosen.

The mathematical structure of a general non-Abelian gauge theory was described in section 1.4. So we can readily substitute to the Yang-Mills Lagrangian (1.31) to get

$$\mathscr{L}_{QCD} = -\frac{1}{4}\sum_{j=1}^{8} F^j_{\mu\nu}F^{\mu\nu j} + \sum_{q=u,d,c,s,t,b} \bar{q}(i\not{D} - m_q)q$$

where $\not{D} = \gamma^\mu D_\mu$ and covariant derivative is defined (cf. (1.26))as follows

$$D_\mu = \partial_\mu - ig_s G_\mu = \partial_\mu - ig_s \sum_{j=1}^{8} G_\mu^j t^j$$

where g_s is coupling constant of the strong interaction and G_μ^j are vector fields introduced to maintain local gauge invariance. In this case they are called gluons. Matrices t^j are generators of the $SU(3)$ group and are called Gell-Mann matrices:

$$t^1 = \begin{pmatrix} 0 & 1 & 0 \\ 1 & 0 & 0 \\ 0 & 0 & 0 \end{pmatrix}, \quad t^2 = \begin{pmatrix} 0 & -i & 0 \\ i & 0 & 0 \\ 0 & 0 & 0 \end{pmatrix}, \quad t^3 = \begin{pmatrix} 1 & 0 & 0 \\ 0 & -1 & 0 \\ 0 & 0 & 0 \end{pmatrix},$$
$$t^4 = \begin{pmatrix} 0 & 0 & 1 \\ 0 & 0 & 0 \\ 1 & 0 & 0 \end{pmatrix}, \quad t^5 = \begin{pmatrix} 0 & 0 & -i \\ 0 & 0 & 0 \\ i & 0 & 0 \end{pmatrix}, \quad t^6 = \begin{pmatrix} 0 & 0 & 0 \\ 0 & 0 & 1 \\ 0 & 1 & 0 \end{pmatrix},$$
$$t^7 = \begin{pmatrix} 0 & 0 & 0 \\ 0 & 0 & -i \\ 0 & i & 0 \end{pmatrix}, \quad t^8 = \frac{1}{\sqrt{3}} \begin{pmatrix} 1 & 0 & 0 \\ 0 & 1 & 0 \\ 0 & 0 & -2 \end{pmatrix}$$

It is easy to verify that these matrices obey commutation relation

$$\left[t^a, t^b\right] = i f^{abc} t^c$$

where the structure constants f^{abc} are totally antisymmetric in their indices and the only non-zero components are

$$\begin{aligned} f^{123} &= 2 \\ f^{147} = -f^{156} = f^{246} = f^{257} = f^{345} = -f^{367} &= 1 \\ f^{458} = f^{678} &= \sqrt{3} \end{aligned} \tag{1.93}$$

The components of the field tensor $F_{\mu\nu}$ are

$$F_{\mu\nu}^j = \partial_\mu G_\nu^j - \partial_\nu G_\mu^j + g_s f^{jkl} G_\mu^k G_\nu^l$$

Because of the non-Abelian nature of $SU(3)$ group we can see that $\mathscr{L}_{QCD}$ contains gluon-gluon coupling and the gluons carry the colour charge. Thanks to this fact, QCD enjoys two very important properties which cannot be found in Abelian theories like QED. This properties are asymptotic freedom and quark confinement.

The asymptotic freedom in short means that the interaction between quarks can be arbitrary weak at ever shorter distances (i.e. when the length scales converge to zero or equivalently energy scales are arbitrary large). It was discovered by D. Gross, F. Wilczek and D. Politzer in 1973.

This phenomenon can be intuitively explained in terms of screening and antiscreening. Let us consider a field of virtual charged particles (for example electron-positron pairs in the vacuum). If we put for example a positive charge in this field it will repel the positrons from the surrounding electron-positron pairs. When looking from distance the remaining electrons will cancel the field of this charge - thus the name screening. However, if we go closer and closer to this charge, we will see less and less effects from the virtual particles, so that the effective charge will increase. Exactly this happen in QED.

The same effect will appear with colour charge and virtual quark-antiquark pairs. But, unlike in QED, the force carriers (gluons) themselves are charged. And because they carry colour charge in a different manner than quarks (roughly speaking, they carry some combination of colour and anticolour), the gluons do not screen the central charge but are acting in rather opposite way. This is called antiscreening. Thus, when we come closer to the central charge it becomes weaker and weaker.

The question is, which effect wins? For three colour QCD the winner is antiscreening as long as we do not have more than 16 different flavours of quarks (today we know six). This means that in smaller and smaller distances the strong interaction could be arbitrary weak.

The existence of the asymptotic freedom allowed the usage of a perturbation theory to make highly precise prediction of experiment results - these from LEP did not differ more than a few per cent.

The other property, quark confinement, could be understand as the other face of asymptotic freedom. It states that the colour potential between two quarks increase linearly with their distance. Although it has not been analytically proven so far, it explains why we are not able to see free quarks: when we try to separate them, their binding energy increases until there is enough energy to create a quark-antiquark pair which recombines with original quarks to form new hadrons.

Since its creation in early 1970s, the QCD has successfully undergone a lot of experimental testing, culminating in verification of perturbative QCD at LEP. However there are still unsolved problems mostly in areas which cannot be described by perturbative QCD. This is for example one state of a quark matter called quark-gluon plasma, where the quarks and gluons are expected to be unconfined. If this state of matter really exists we should be able to create it at LHC. The experiment ALICE is designed to study exactly this phenomenon.

Chapter 2

High Energy Physics Experiments

2.1 CERN

The development of our understanding of the Universe would be unthinkable without an experiment. In the field of particle physics we try to study objects which do not behave according to our macroscopic experience, so the experiment is really essential. Last century showed us many occasions when the well interpreted experimental result completely changed our view of the microscopic world. For instance it was the discovery of the atomic nucleus and of the neutron.

The most common scheme of the particle physics experiment is to make particles collide and study what happens - the first experiment of this type was carried out by E. Rutherford. His setting has however a big disadvantage: because of the conservation of the momentum of the center of mass, large portion of energy of the scattered particles cannot be used in collision. Hence today we prefer to collide two particles moving in opposing directions in such way that their common center of mass is stationary, so that all energy is used during collision.

In the late 1940s it was clear, that particles coming out of radioactive decay or from cosmic rays have insufficient energies for further research, so the new powerful accelerators were constructed in the United States. Those required huge teams of scientists and engineers as well as generous funding. Because no single European country (especially in the afterwar years) could compete with this, it was suggested to create a joint European laboratory for particle physics. In 1952 eleven governments set up a provisional "Conseil Européen pour la Recherche Nucléaire", which was dissolved in 1954 after the creation of the European Organization for Nuclear research, but its acronym (CERN) has remained in use until today. The CERN is

located at the Franco-Swiss border near Geneva and today it has 20 member states, most of them from the EU, Switzerland and Norway being the notable exceptions.

In 1959 the CERN's first major machine - 28 GeV Proton Synchrotron (PS) - was finished, thus becoming the most powerful accelerator of that time. However, due to the laboratory's practice of linking accelerators it is still in use. The next large accelerator is 300 GeV Super Proton Synchrotron (SPS) which was completed in 1976. Soon after its completion it was converted from proton-proton collider to the proton-antiproton collider. In 1983 the long-sought $W^{\pm}$ and Z bosons were discovered at this machine, thus confirming the predictions of the GWS Standard Model. In 1989 the Large Electron-Positron collider (LEP) was started. With its circumference of 27 km it became the largest scientific instrument ever built. The positron and electron beams were at first prepared and accelerated in the PS and SPS and after that they were injected into LEP, which further increased their energy up to the 50 GeV. This allowed productions of Z bosons ($m_Z = 91$ GeV) during collisions. In the second half of 1990s the LEP energy was increased to the 100 GeV, thus making production of $W^{\pm}$ pairs possible. The LEP was in operation for 11 years and its highly precise measurements confirmed the Standard Model in the extraordinary fashion.

In 1994, CERN council approved the construction of the Large Hadron Collider (LHC). It will be the first CERN machine constructed with substantial material and financial contribution from non-member countries. For instance, the machine hardware is being constructed in Canada, India, Japan, Russia and in the United States. LHC is planned to start operation in the middle of 2007.

2.2 LHC

The LHC is being constructed in the old LEP tunnel which is buried from 50 to 175 m underground. Although the LHC will be the most powerful scientific instrument ever built, the basic experimental scheme has not change since the time of Rutherford - one particle (or today rather a beam of particles) collides with some other and we measure the outcome. The LHC is designed to collide beams of protons (center of mass energy up to 14 TeV) and the beams of heavy ions, like lead nuclei (center of mass energy up to 1150 TeV). It will be the last link in the CERN's accelerators chain (see figure 2.1[1]). The proton beams will be prepared in the PS and further accelerated in the SPS until they reach the energy of 450 GeV. After that they will be injected into the LHC which will increase their energy up to 7

[1]Figure taken from [9]

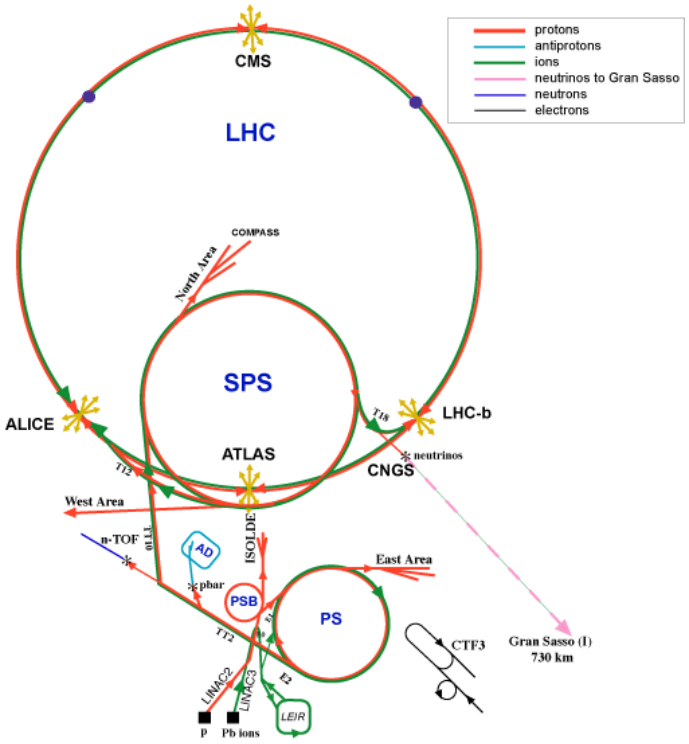

Figure 2.1: Chain of the CERN accelerators

TeV per beam. From the technical point of view, the LHC is (as all big modern accelerators) a synchrotron. This means that it uses variable magnetic and electric field to keep particles on the constant track. Contrary to the LEP, the synchrotron radiation is not significant at LHC, due to the large masses of accelerated particles.

The beams will be running in separate pipes in opposing direction (see figure 2.2[2]) for LHC tube cross section). Because each beam will carry the same charge, the only way to make them run in opposite directions is to have differently oriented magnetic field in each pipe. However, there is not enough place in the LEP tunnel to install two separate rings of magnets, so the LHC will use twin bore magnets with two sets of coils and two beam channels sharing the same mechanical structure.

Besides energy, the other important parameter which decides the outcome of the

[2]Figure taken from [11]

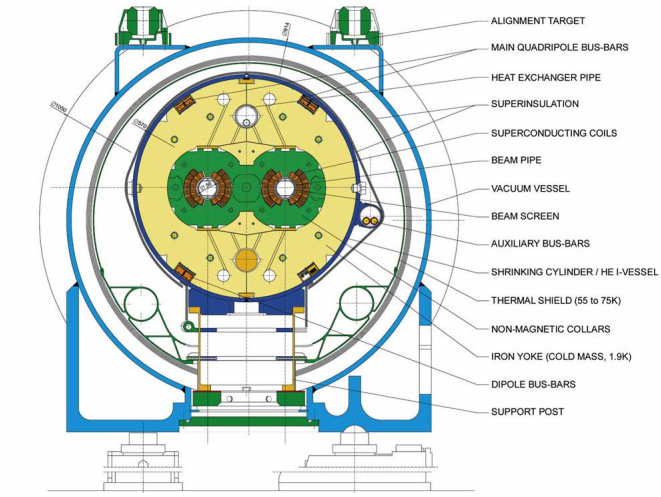

Figure 2.2: Cross section of the LHC tube

experiment is the luminosity L. It is defined as

$$N_{event} = L\sigma_{event} \tag{2.1}$$

where σ_{event} is the cross section of studied collision and N_{event} is the number of events. Because with the energy the De Broglie wavelength decreases like 1/E and consequently the cross section decreases like $1/E^2$, the luminosity must increase to maintain the same efficiency of the physics programme. The LHC aims at the luminosity of $10^{34}\text{cm}^{-2}\text{s}^{-1}$, which is about 100 times higher than any other accelerator in the present or past. It will be achieved by preparing high-density beams at PS and SPS: each beam will consist of 2835 bunches of 10^{11} particles each. They will be separated by 25 ns. This will result in rather large beam current (0.53 A) which will require intense magnetic field. This will be secured by superconductive magnets operating at temperature of about 2 K.

The LHC contains also eight regions, where there are no magnets, i.e. the particles run straight there, sharing the same pipe. These areas are called insertion regions (IR) and inside them there are interaction points, where the beams can collide. At this sections the LHC experiments are located (see figure 2.3[3]) for LHC layout). However, only a tiny fraction od particles collides head-on when two bunches cross at the interaction point. Most of them are deflect by the strong electromagnetic field

[3]Figure taken from [13]

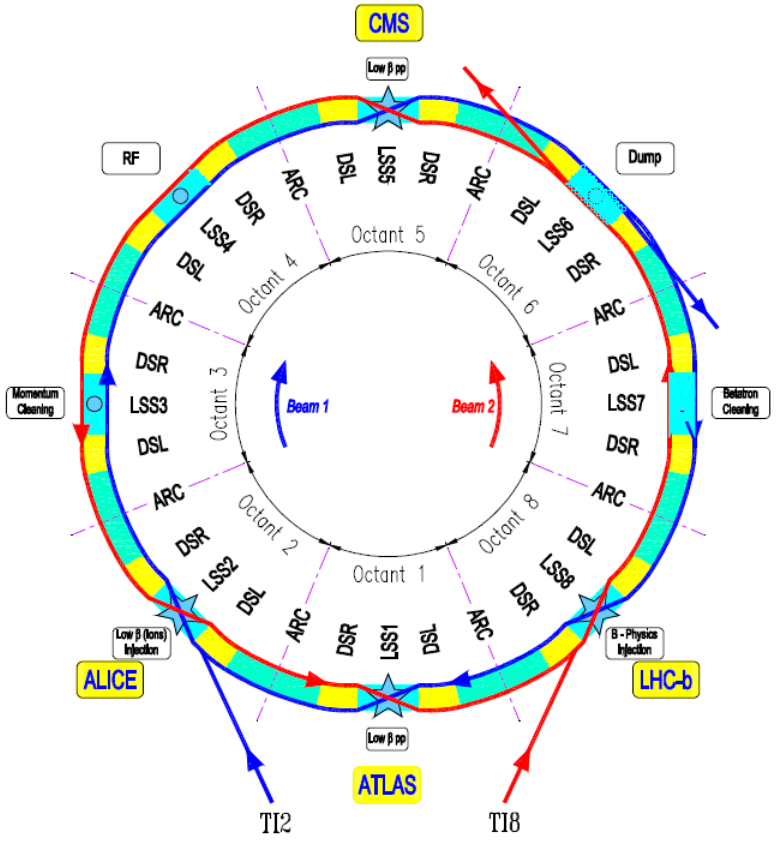

Figure 2.3: Layout of the LHC

of the opposing beam. This effect is stronger for denser bunches and accumulates turn after turn, leading ultimately to the beam loss. This sets certain critical limit for bunch density, which we cannot cross if we want to maintain a reasonable lifetime of the particle beam. The PS and SPS are set so that they produce beams with particle density close to the critical one. The result is that LHC will have around 20 collisions for each bunch crossing.

The accelerated beams will be stored for about 10 hours, meaning some 400 million revolutions around the machine. During that time, the beam quality will degrade - partly because of interaction with the other beam and partly due to chaotic behaviour of particles caused (among other) by nonlinear components of guiding and focusing magnetic field. Because there is no theory to predict their behaviour, robust

Table 2.1: LHC Statistics

particles used	protons and heavy ions (Pb^{82+})
circumference	26.659 m
injected beam energy	450 GeV (protons)
beam energy at collision	7 TeV
magnetic field at 7 TeV	8.33 Tesla
operating temperature	1.9 K
revolution frequency	11.2455 kHz
power consumption	120 MW

simulations are used do determine the tolerances for the quality of magnets. Despite all this, a fraction of particles will diffuse towards the wall, converting their energy into the heat. This could induce a quench in the superconductive magnets and so interrupting the operation for hours. To prevent this, the collimation system will catch the unstable particles before they would be able to reach the wall.

In the preceding paragraphs there were briefly outlined the main challenges the constructors of the LHC have to deal with. Most of them are caused by the fact that the LHC combines for the first time in history the large beam current at very high energy with the sophisticated superconductive technology. Also fitting the LHC into the tunnel which was build for less powerful machine is not without problems. The vital statistics of the LHC are summarized in table 2.1.

2.3 Physics at LHC

The main reason, why the LHC is being built, is to discover the Higgs boson (and thus prove GWS Standard Model) and to discover supersymmetric particles (if they exist). It is also possible, that there is not just one Higgs boson, but a whole family of them. Namely, according to the Minimal Supersymmetric extension of the Standard Model (MSSM), there are four Higgs particles ($H^{\pm}$, h, H and A).

However, there are plenty of other lines of research in which the LHC can participate. Even at initial lower luminosity (with the order of magnitude of $10^{33}\mathrm{cm}^{-2}\mathrm{s}^{-1}$) the LHC will operate as a b-quark and t-quark factory, producing approximately 10^7 top-antitop pairs a year. This will allow us more detailed study of this heavy quarks, particularly precise measurements of the top quark mass. So far the only

machine capable of producing top quarks has been the Tevatron in the Fermilab, USA. The latest result[4] from Tevatron is $m_t = 172.7 \pm 3.5$ GeV. The LHC can also provide detailed study of B-physics, i.e. the decay of B-mesons - bounded states of b-quark and some other quark. These are of particular interest because they will tell us more about possible mechanisms of CP-violation. The $b\bar{b}$ year production rate will be about $10^{12} - 10^{13}$, so the main problem will be to trigger and select interesting decay modes.

The LHC will also allow us to study SM physics like QCD and electroweak interactions. Very interesting seems to be the study of deconfined quarks during the state of quark-gluon plasma, which will result from the collision of heavy ions.

Last but not least, the LHC has the capability to produce also events which are not described by present-day SM, so if SM is just an effective theory for low energy scales (which seems probable, cf. discussion at the end of the paragraph 1.5.5), the LHC could give us a clue to some more comprehensive theory.

2.4 LHC Experiments

There are five experiments dedicated to measuring the outcome of the LHC collisions:

ATLAS (**A** **T**oroidal **L**HC **A**pparatu**S**) is a general purpose detector designed to exploit the full LHC potential. It is being built at Point 1 (see fig. 2.3). The project involves collaboration of more than 1800 scientists and engineers from 34 countries. Although ATLAS main task is to search for the origin of spontaneous symmetry breaking in the electroweak sector of the SM, it is designed to measure the broadest possible range of signals. Because of unprecedented energy and collision rate of the LHC, the ATLAS will be larger and more complex than any other detector. The main lines of the ATLAS research are:

- The search for the Higgs boson or any other mechanism of the electroweak symmetry breaking
- The investigation of CP violation in B-decays
- The precise measurement of mass of heavy particles like top quark or W boson

[4] October 2005, [12]

- The search for supersymmetric particles or any other new models of physics
- The studies of compositeness of fundamental fermions

To fulfil these goals the ATLAS consists of several components which together provide the full information about the collision. These subdetectors will be described later.

CMS (**C**ompact **M**uon **S**olenoid) is also a general purpose detector. The name "compact" means that it is somewhat smaller than ATLAS (about 8 times in volume), but has about twice its weight. It is being built at Point 5 (cf. fig. 2.3) - unlike ATLAS it is being assembled on the surface and lowered to the experimental cavern afterwards. The name also signalizes that CMS is optimized for tracking muons and its magnet will be the largest solenoid ever built, producing a magnetic field of the strength of 4 Tesla. The CMS collaboration involves about 2000 scientists and engineers from 36 countries. The scientific goals of the CMS are similar to that of ATLAS, namely

- The search for origin of the spontaneous symmetry breaking (Higgs boson)
- The search for physics beyond the SM - for example supersymmetric particles
- The study of heavy ion collisions and of the formation of the quark-gluon plasma, emulating thus the very first moments after the Big Bang

Although the construction of two similar detectors may seem as a waste of time and money, it fulfils the natural requirement on experimental physics - that any result should be independently confirmed. This helps reduce systematic as well as random errors.

ALICE (**A** **L**arge **I**on **C**ollider **E**xperiment) is a detector specially designed to study the collisions of heavy ions. Experiments in the CERN in 1990's and in the Brookhaven National Laboratory, USA, in 2000's showed that at very high temperatures the quarks are not confined inside hadrons but they are are rather free in a state which was called the quark-gluon plasma (QGP). It is supposed that this state of matter exists naturally inside the quasars and that it was also one of the initial stages of the Universe.

The LHC should create the quark-gluon plasma by colliding nuclei of lead with an energy of 5.5 TeV per nucleon. The QGP will be then identified thanks

to the specific signatures of leaving particles - for example the production of strange particles and the suppression of the production of J/ψ mesons (made from charm and anticharm pair of quarks), because the turmoil of QGP prevents forming of heavy quark pairs.

ALICE is being constructed at Point 2 and its collaboration involves more than 1000 people from 28 countries.

LHCb (**L**arge **H**adron **C**ollider **b**eauty) is an experiment devoted to the measurement of CP violation. It is expected that it could be most clearly seen in the difference between the decay of Bd meson ($d\bar{b}$) to J/ψ ($c\bar{c}$) and K^0 ($d\bar{s}$) and the decay of anti-Bd meson to respective antiparticles. By studying the difference in the decay times, we would be able to determine the complex phase of CKM matrix.

This type of experiment has been already tried (among others) at the LEP, SPS or Tevatron. Nevertheless, none of these machines produced enough b quarks to observe such a subtle effect like CP-violation. The LHC is able to produce much more b quarks than previous accelerators, thus hopefully making the observation of CP-violation possible.

The LHCb is located at Point 8. This experiment has nearly 900 participants from 13 countries.

TOTEM (Total Cross Section, Elastic Scattering and Diffraction Dissociation at the LHC) is an experiment dedicated to the measurement of the total cross section, elastic scattering and diffractive processes at the LHC. Because its measuring method is luminosity independent, the results obtained during initial lower luminosity runs will be used as a reference for the normal LHC runs.

The TOTEM is a small experiment which does not require any special infrastructure so it is integrated with the CMS in the Point 5. More than 50 scientists from 9 countries participates at this experiment.

Chapter 3

ATLAS Detector

3.1 Introduction

The most prominent quest of the ATLAS experiment is to find Higgs boson (or "something similar" which will cause the spontaneous breaking of the electroweak symmetry), as well as observe the behaviour of particles in the region of very high energies (above 1 TeV) that could give as a clue which of the proposed extensions of the Standard Model describes most correctly the Nature. To fulfil these requirements, the ATLAS has to be as complex as possible to measure everything which is coming out of the proton-proton collision.

The overall picture of the detector and its main subsystems could be seen at fig. 3.3[1]. Whole detector is set into a strong magnetic field generated by the central solenoid magnet as well as by air-core toroid magnets on the perimeter (in the barrel area and in both endcaps - cf. Appendix and figure 3.3).

The innermost part is called Inner Detector - it measures the tracks of particles immediately after the collision. There are three types of subdetectors: the impact area is surrounded by highly precise semiconductor trackers (pixels and silicon strips) and by less precise straw tracker which, however, gives large number of hits. Inner detector also measures the momenta of particles from the position and time of hits.

Having left the Inner Detector, particles come to the electromagnetic calorimeter - it absorbs photons and light charged leptons, and so it measures their momentum. This could (combined with the information from the Inner Detector - leptons have bent track, while photons go straight) identify the particles.

Energy of hadrons is measured in hadronic calorimeter. Its main task is to

[1]Figures 3.3 and 3.4 taken from [11]

measure energy and direction of hadron jets created after the collision. Of high importance is also the measurement of missing energy - it helps identify non interacting particles like neutrinos.

The outermost part of ATLAS is muon spectrometer. It was designed to fully exploit the potential offered by the superconducting toroid magnets, i.e. to provide precise measurements of muon tracks and momentum. The scheme of particle identification is at figure 3.1[2].

The computing is crucial part of the whole experiment. ATLAS will produce huge amount of data and only a small fraction of them will describe interesting events. The decision which data to throw away and which to leave for further analysis is made by the ATLAS trigger. It is organized in three levels (LVL1, LVL2, LVL3). LVL1 accept data at frequency of 40 MHz and then uses the reduced-granularity data from the subset of detectors to choose regions where interesting events happened. This reduces the data frequency to some 10 - 100 kHz. Second level then uses full-granularity full-precision data from most of the detectors, but examining only the regions identified by LVL1. Data rate is reduced to 100 Hz - 1 kHz. Last level uses full data for selection of events which will be stored for offline analysis. Events are stored with a frequency of 10 - 100 Hz.

Afterwards, the raw data acquired from the detectors are used to reconstruct the events. There are several reconstruction algorithms (each using data from different set of detectors) and they all use a common software framework called Athena (for more details cf. Appendix). Reconstructed events are then stored in the form of ROOT ntuples that are subsequently used for further study. Such an analysis was also subject of this thesis (see chapter 4).

3.2 Requirements on detector performance

It is not clear what kind of Higgs physics will be discovered by LHC. There could be one Standard Model Higgs boson, five of them as proposes the Minimal Supersymmetric Extension of the Standard Model (MSSM), or some more exotic scenario would happen. Even if Standard Model is correct and there is only one Higgs boson, there are several decay modes depending on its mass, so the detector has to be prepared for all possibilities.

Although the Standard Model cannot predict the mass of Higgs boson, it could give some limits to it. If we want our theory to be consistent for example to the scale of 10 TeV, the Higgs mass should not be lower than 130 GeV and not higher

[2]Figure taken from [11]

than 190 GeV. If we increase the scale, the allowed area is narrower and vice-versa. Therefore, a discovery of very light Higgs would suggest that there exists some new physics below 10 TeV, i.e. already in the region reachable by LHC.

The main production mechanism of Higgs boson at the LHC will be gluon fusion and the dependance of branching ratio of various decays on Higgs boson mass could be found at fig. 3.2[3]. For lower Higgs mass the decay to $b\bar{b}$ is dominant, while at higher masses it decays preferably to heavier particles like W^+W^- or ZZ pairs. These would however quickly decay to leptons. Therefore the clearest signature of Higgs at LHC would be $H \to ZZ \to 4\ell^{\pm}$ for Higgs mass greater than 130 GeV. Nevertheless we should also mention the decay to the photons: although its branching ratio is about a per mile, it has a distinctive final state, so it could be exploited quite well.

All these processes have large background (in case of light Higgs and the decay to $b\bar{b}$, the Higgs signal is several orders of magnitude fainter than the background), so the ATLAS has to be as precise as possible to be able to find Higgs boson. This means excellent performance at momentum and energy measurement, as well as ability to locate secondary vertex and measure the charged leptons tracks (in the case of $H \to ZZ \to 4\ell^{\pm}$).

In case of the MSSM, two Higgs doublets are required, resulting in five physical states: charged doublet H^+, H^-, neutral lighter scalar h, neutral heavier scalar H and neutral pseudoscalar A. They can be explored among others in decays $A/H \to \tau\tau$, which will require very good τ identification and missing energy resolution.

High resolution secondary vertex identification, efficient charged particle track reconstruction and lepton identification will be also necessary for B physics studies as well as for measurement of top quark properties.

To sum up, ambitious ATLAS physics programme requires both high resolution tracking (this will be task of Inner Detector and muon spectrometer) and precise energy measurements performed by ATLAS calorimetry.

3.3 ATLAS components

3.3.1 Inner detector

The Inner Detector measures tracks of all charged particles created in pp collisions. The core of Inner Detector form three layers of highly precise silicon semiconductor trackers called pixel detectors. Most of them are placed in three cylinders (barrel

[3]Figure taken from [21]

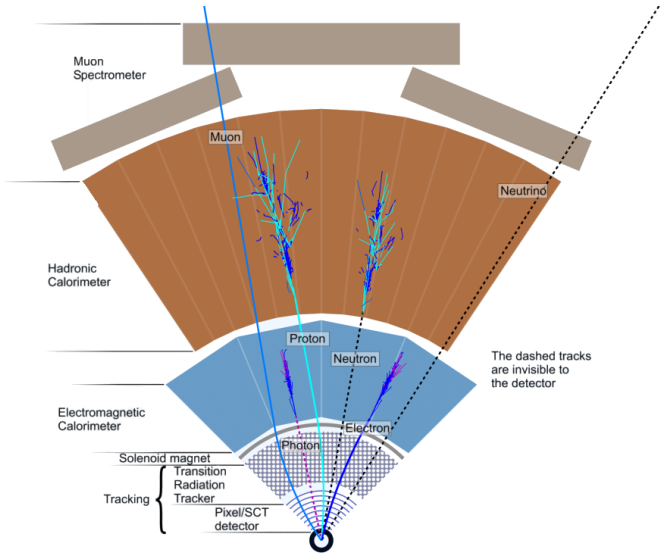

Figure 3.1: Basic scheme of particle identification

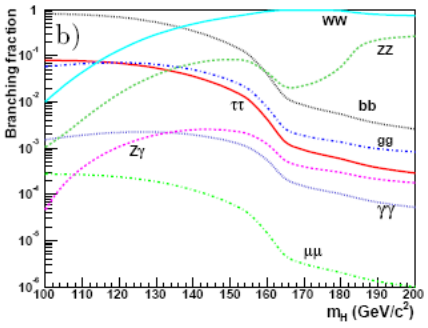

Figure 3.2: Branching ratio of various SM Higgs decays

area), some of them are also placed on the disks perpendicular to the beam direction (see fig. 3.4). Together they cover the pseudorapidity area of $|\eta| \lesssim 2.5$ (cf. Appendix).

Because each layer causes dissipation of energy (not to mention their high cost) the number of pixel layers is limited. The three pixel layers are reasonable compromise. Pixels have very high granularity, so they offer measurements of exquisite precision in both $R-\phi$ and z direction. There are about 1.4×10^8 pixel elements, each of them has size 50×300 μm and they are mounted on 1744 pixel modules (1456 in barrel and 144 in each end-cap). The resolution is 14 μm in $R-\phi$ direction and 87 μm in both z and R direction.

The second type of detector through which the particles pass are silicon strips. Together they are called semiconductor tracker (SCT). They are in many aspects similar to the pixels, however, they differ in the granularity in z direction. Therefore, they offer precise measurements in $R-\phi$ direction, but have lesser resolution in z direction. They are 75 or 112.5 μm wide and 12 cm long. The resolution in $R-\phi$ is comparable with the pixels (15 μm), but in the z direction it is much worse, namely 770 μm.

The third subsystem of the Inner Detector is the transition radiation tracker (TRT). It is composed from 370 000 straw detectors (50 000 in barrel and 320 000 in the end-caps). Electron identification capability is enhanced by xenon gas which

Table 3.1: Inner Detector parameters

System	Element size	Resolution	η coverage
Pixels	50 $\times$ 400 μm	$\sigma_{R\phi} = 14$ μm $\sigma_z = 87$ μm $\sigma_R = 87$ μm	$\pm$ 2.5
SCT	75 or 112.5 μm $\times$ 12 cm	$\sigma_{R\phi} = 15$ μm $\sigma_z = 770$ μm	$\pm$ 2.5
TRT	4 mm diameter 150 cm long	$\sigma_{R\phi} = 170$ μm per straw	$\pm$ 2.5

is set between and inside the straws. It detects the transition radiation photons which were created by passing-by highly energetic particles and so it can distinguish between the electrons and hadrons because each creates a different number of these photons.

The TRT is designed to give large number of measurements over a long track length, namely over 36 hits produced by about 64 layers. Each straw has 4 mm in diameter and the length of 150 cm. The resolution is 170 μm in $R-\phi$ direction and 150 cm in z direction.

The combined hits from pixels, SCT and TRT are then used by some reconstruction software (typically within Athena framework) to compute the particle trajectory and momentum. Main characteristics of the Inner Detector are summarized in the table 3.1.

3.3.2 Calorimetry

The LHC physics programme impose high demands on the measurement of energy. In particular, ATLAS calorimeter has to be capable of reconstructing the energy of electrons, photons, and hadrons, as well as measuring the missing transverse energy (and therefore identify neutrinos).

ATLAS calorimeter consists of two parts: the smaller inner part is the electromagnetic calorimeter, designed to measure the energy of electrons and photons. It is build from a number of absorber plates between which is a liquid argon. Absorber plates are made from lead and steel, and they cause the passing high-energy electron or photon to decay to shower of less energetic electrons and positrons. These cause ionization of molecules of liquid argon, thus creating electrical current which is then

detected on copper electrodes. The energy of particles to which original electron decayed can be calculated from the value of this electrical current. Comparing to the momentum which was measured by the Inner Detector we can calculate also the amount of missing transverse energy.

Hadronic calorimeter (also called tile calorimeter) is made from steel absorbers and scintillating plates. Like in the LAr calorimeter, the interaction with absorbing material cause hadrons to decay to the lighter particles. Subsequently the light produced by scintillating plates is measured.

Because processes involving Higgs boson are extremely rare, the calorimeter should have large rapidity coverage. That is achieved by having full segmentation for $|\eta| < 2.4$ and coarser segmentation for $2.4 < |\eta| < 3.2$. Hadronic calorimeter has even larger acceptance: $|\eta| < 5$ - this allows studies of proposed supersymmetric particles.

3.3.3 Muon Spectrometer

Precise muon measurement is a crucial part of ATLAS experiment. Such a demand follows from the above mentioned physics programme, particularly from the decays like: $H \rightarrow ZZ^* \rightarrow 4\ell$. Also the total energy of particles could not be measured correctly if we would ignore muons. Therefore the spectrometer has high resolution ($\sim 60\ \mu$m) over the momentum range from 5 GeV to more than 1 TeV.

The muon spectrometer is in fact very large straw tracker similar in function to the TRT in Inner Detector. It forms the outermost part of ATLAS detector - its inner and outer radius are 5 m and 10 m, respectively. Such a tremendous size is necessary because muons easily penetrate through all other parts of the ATLAS. That is why muon spectrometer serves also for simple identification of muons - practically no particles of other types are able to pass the calorimeters and leave signs at muon spectrometer (neutrinos are able to pass, but they do not leave any signs anywhere - they are detectable only from missing energy).

In the barrel area there are three layers of muon chambers (precise Monitored Drift Tubes - MDT and fast Resistive Plate Chambers -RPC) mounted on the toroid air-core magnets. In the region of end-caps, there are also three layers - mounted vertically on discs perpendicular to the beam axis. Precision measurement is done by MDTs and by more radiation tolerant Cathode Strip Chambers (CSC) that are in areas of high pseudorapidity $|\eta| > 2$ and on the innermost disc.

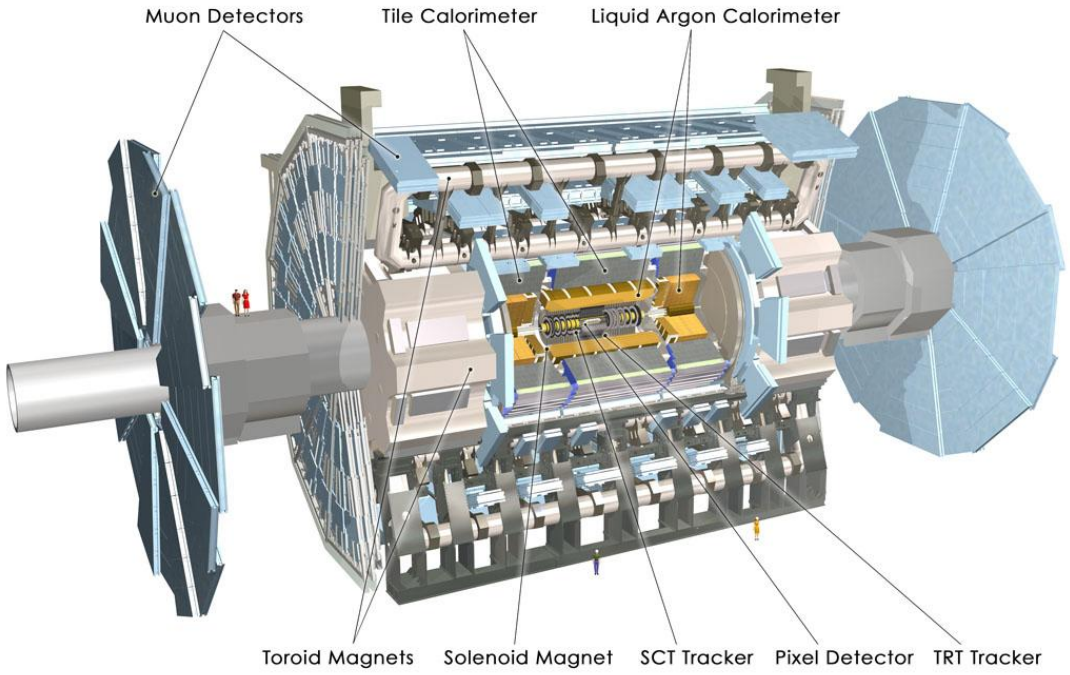

Figure 3.3: ATLAS detector

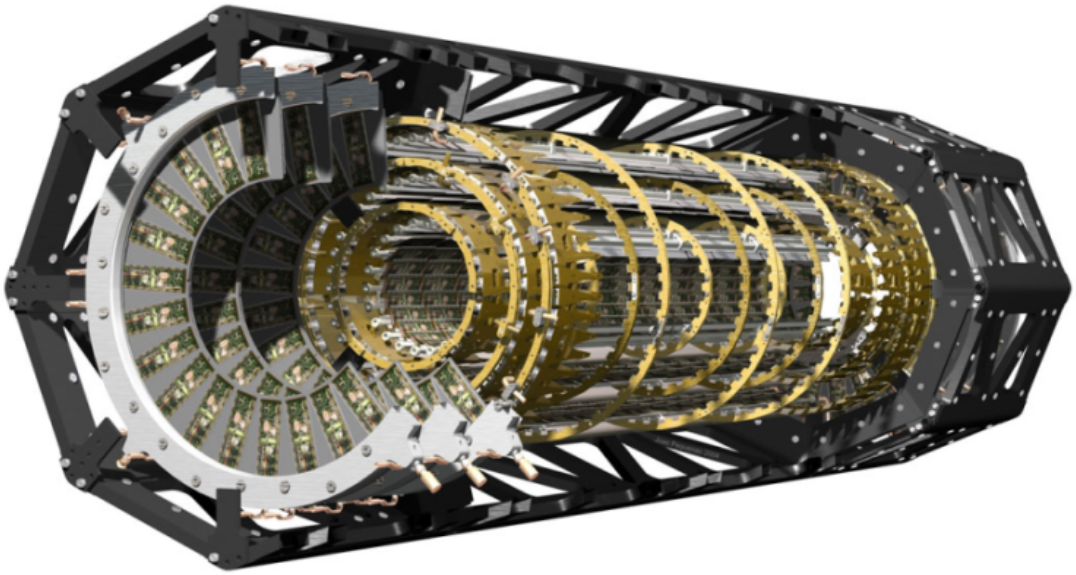

Figure 3.4: Pixel detector

Chapter 4

Calibration of the ATLAS Inner Detector

4.1 Introduction

Previous chapters showed that precise tracking is absolutely necessary for identifying the particles created in pp collisions at LHC, as well as for measuring their properties. However, there are several things limiting our ability to find proper tracks. First of them is the intrinsic resolution of the Inner Detector (Pixels and SCT, details given in tab. 3.1). It is a given, unchangeable value resulting from the design of detectors.

On the contrary, the other two effects depends on how the Inner Detector is assembled. First of them is module misalignment, i.e. the precision with which we know the position. Note that the important thing is not the very value of module deviance from the nominal position, but rather the precision of our knowledge of this deviation.

The last significant cause of uncertainties are module shape distortions (most important from them being the bows of module staves in barrel area). Nevertheless we are able to determine both misalignment and shape distortions, and as a result we can get rid of their effects. The way how to do that will be described in this chapter.

4.2 Alignment of the SCT and pixel detectors

4.2.1 Basic concepts

We may be interested in two issues concerning the alignment of pixel and SCT modules: how well we have to know their position to degrade intrinsic detector resolution in as small way as possible, and how well we would know their positions before the data-taking begins. Previous studies [26] answer the first question: our knowledge of module positions will have to better than 7 μm for pixels and 12 μm for SCT in order that misalignment do not degrade the intrinsic resolution more than 20 %. This precision could be achieved with a statistics collected from a few-day run, however the full understanding of associated systematics would take months.

The second question may not seem as important as the first, but the contrary is the case - the answer would tell us if we would be able to find any tracks at all in the beginning. This was discussed in great detail in a study [25].

Because we already have some experience from mounting the modules on the staves, the main concern of [25] was to find if the "as-built" precision will be good enough and also whether some affordable improvement in assembling would lead to a significant increase in detector performance. That study considered only pixels and SCT because TRT will not be used in the initial alignment.

The idea of the survey of misalignment effects is following - we use the data from direct measurement of module deviations to define a set of misalignment constants - different for pixels and SCT as well as for different regions of Inner Detector (for example, pixel endcap modules are mounted with greater precision than these in barrel area). These constants were then used to build a misaligned detector geometry during the reconstruction of tracks using `iPatRec` algorithm, while the simulation of hits remained unchanged. The results were subsequently compared with these obtained for unchanged, i.e. perfect geometry.

Several sets of misalignment constants were used: some of them reflecting the best expected uncertainties in module assembly - 50 μm in pixel barrel, 25 μm in the pixel endcaps, 100 μm in SCT barrel and about 50 μm in SCT endcaps. Other sets introduced larger displacements in various directions to find out how sensitive the track reconstruction is. Also two types of shifts were used: a displacement of a complete layer of module with respect to the others, and a random displacement of modules within one layer. Most of the sets used either the displacements of pixels modules or of SCT modules, however, few of them combined shifts in both parts to determine which of them has bigger effect on tracking resolution.

Detector performance was characterized by the track finding efficiency and the

fake track rate (this will tell us how easy is to find a track), and by the deterioration in the detector resolution (this will tell us how good will be the detector at doing some discovery-type physics).

For reconstruction following data sets were used:

- single muon events with an energy of 5 GeV (representing initial alignment) and 200 GeV ("discovery type" muons)
- dijet events with an energy of 17 GeV - typical low luminosity event from an early ATLAS run giving a reasonable high track density
- Higgs production associated events - these represent highly demanding track recognition

4.2.2 Results

Two sets of misalignment constants were used to describe pixel modules. The first of them (P1) described the expected initial alignment. Studies of the reconstructed tracks showed that the first case leads to a few-percent degradation in a trackfinding efficiency (the exact criteria for recognizing the tracks can be found in [25]) and to about 25-50 % degradation in the tracking resolution.

The second set of constants (P2) represented considerable layer-layer misalignment (50 μm in contrast to maximum 20 μm expected from the direct survey) and also the displacement within the layer was doubled with respect to the set P1. Comparison of the reconstructed tracks with these using perfect geometry showed that such a misalignment causes deterioration in trackfinding efficiency (10-15 %) and practically 100 % degradation in the resolution. The study of the dependence on the pseudorapidity η and polar angle ϕ showed that efficiency drop is larger in the barrel region and that there is no visible dependence on ϕ.

The SCT modules were also at first studied using the constants describing the as-built misalignment (set S1). In contrary to pixels, this misalignment led to the about 20 % degradation in trackfinding efficiency. The resolution was worsen by a factor of two. Similarly to the pixels, this effects are worse in the barrel than in the endcaps. Also a dependence on a polar angle ϕ was found: it is easier to reconstruct tracks in the vertical direction than in the horizontal one. This phenomena seems to be a general feature of misaligned SCT - this was verified by using other sets of constants generated with different random number seed.

Other two sets of constants tried to find out whether we would get better results if the positions of SCT modules were determined somewhat better than it is expected. However, the acquired gains in efficiency and resolution were rather negligible.

Several other sets of constants were used to investigate the sensitivity of track reconstruction on misalignment in various direction. The result was that barrel modules are very sensitive to any displacement in r direction while the endcap modules are insensitive to any moves in z direction as large as 500 μm.

The last three sets described combined misalignments in both pixels and SCT. First of them represented as-built misalignments, i.e. combined P1 and S1. The performance was only slightly worse (about 1 - 2 %) than S1 alone. Nevertheless, for bigger SCT misalignments, the relative effect of displaced pixels on resolution also grew (5-8 % in trackfinding efficiency and resolution was degraded by additional 25 %).

Above studies investigated the performance lost directly - by comparing the resolution with respect to the Monte Carlo Truth before and after the degradation. However, other approach is also possible - using track refitting. This means that the original track is being refitted twice - for the first time using perfect alignment and for the second time, using above mentioned misalignment constants, i.e. the pattern recognition (converting raw data to position of hits) is done only once. This isolates the effect of misalignment on tracking resolution from any other effects. For this purpose, tracks found by `xKalman` algorithm were used. Resolution degradation is evaluated by using a factor f expressing ratio between the degradation produced by misalignment and the intrinsic resolution with perfect alignment.

The results quantitatively confirmed these obtained from previous studies. For constants P1 the f has values about 1, i.e. the degradation caused by misalignment is about the same size as intrinsic resolution. This means that resolution is degraded by a factor of $\sqrt{1+f^2} = 1.4$. Nevertheless for other sets of misalignment constants the effect of misalignment grows, reaching value of $f = 27$ for large displacement in r direction of SCT modules. This study also confirmed that endcaps are less sensitive to module misalignments. The results from combined SCT and pixel misalignment were almost the same as for SCT displacement alone.

4.2.3 Conclusions

The following results could be summed up in a following way:

1. The initial trackfinding will be possible with the as-built precision, although it will be somewhat degraded from the state with perfect geometry.

2. SCT appears to be very sensitive to the misalignments in r direction, therefore we must measure this coordinate as carefully as possible.

3. Relaxing the tolerances of assembly precision of current values leads to significant losses in performance, on the other hand, improving our knowledge of SCT modules brings only negligible improvement.

4. The detector performance is much more influenced by SCT misalignments than by these of pixels.

5. The effects of misalignment are larger in the barrel than in the endcaps.

4.3 Module shape distortions

4.3.1 Initial Motivation

Another major cause of the deterioration of the the tracking resolution are the module shape distortions (cf. [23]). An important type of shape distortion in the pixel barrel area are bows. A study based on track refitting (similar to the previous chapter) showed that bows with curvature over 0.0001 mm^{-1} have significant effect on tracking resolution. Although we know the size of bows from the initial survey (see [23]) - typical value is about 0.0002 mm^{-1}, this section shows how to determine their size using other approach - track reconstructions. First reason for such a study is that bows can change their size during ATLAS run due to the mechanical fatigue, humidity, etc., the other is that this method can (in a long run) give much better results than direct survey (it is the same case as in the previous section - sufficiently huge statistics gives better precision than any direct measurement). Though [23] mentions general bows along axis which is rotated by angle Ψ with respect to local x axis, this study considered only bows along the local y.

The difference between local z coordinate of the module plane and the local z coordinate of actual position of the module can be calculated using this formula (see fig. 4.1):

$$\Delta z = \frac{1}{2}\,\rho y^2, \tag{4.1}$$

where ρ is the curvature of the bow (typically 0.0001 - 0.0005 mm^{-1}). Following paragraphs will show, if it is possible to determine such a bow from the fitted tracks.

4.3.2 Effects of bows

At figure 4.1 it can be seen how the bow affects hit information. The view is in a direction of a local x. Dashed line is the nominal plane of a module (i.e. without bow), solid line is the bowed module. The bold line is a track of the particle - because of a small curvature we can consider the track to be (at least locally) a line - distance between the former plane and the bowed plane is smaller than 300 μm. Point 1 is the position of a real hit, but the coordinates of point 2 ("fake hit") are used in reconstruction instead. We also suppose that distance 0-1 and 0-2 are the same. That is correct, because $\mathrm{dist}_{0-1} = \alpha \cdot r$, where r is radius of the bow and α is central angle, if the bow is an arc of a circle. The horizontal distance from the peak of the bow to the fake hit is $r \cdot \sin\alpha$. For the bows of expected curvatures the angle α is always smaller than 0.01 rad, so that $\alpha \sim \sin\alpha$.

This effect - shift of a position of the hit in z direction - means that we will get nonzero z residue which should be a function of a local y. The way how to get its value from the track information stored in the ntuple is revealed later.

An algorithm `InDetAlignNt` by Richard Hawkings was used to reconstruct tracks from six sets of simple muon events. They had energies from 3 to 300 GeV and very wide η range. The reconstruction was done within Athena framework and the resulting ntuple was stored in a form of a ROOT file. Subsequently a ROOT macro was used to generate plots and to compute the bows. This macro will be described in the next section.

The events used in the reconstruction are stored in the following parts of DC2 datasets: 2929, 2865, 2930, 2870, 2920, 2931. At first only a small statistics (6×2 000 events) was used (for faster run), only later the effects of larger statistics (110 000 events altogether) were evaluated. That is why the cylindrical symmetry was used in making plots: all modules sharing the same ring (i.e. global z coordinate) and layer (i.e. radial distance from the center) were put into one plot to accumulate statistics.

From the fig. 4.1 it is obvious that the bow has a significant effect on the size of z residues. Figure 4.2 shows plot of z residues as the function of local y for module without bows. The right mean square (RMS) of z residuals is zero, as expected. But if we look on the same plot for the module with bow (fig. 4.3), we could see something quite different. RMS of z residuals is shifted away from zero and the size of the shift is a clear function of a local y. Because RMS shift as the function of local y is more or less quadratic, we can expect some correlation between the size of the bow of the module and the size of the bow in the plot.

If the curvature is taken from the plot (i.e. quadratic coefficient of the quadratic

fit), the resulting number is somewhat smaller than the real physical bow of the module. For example the curvature computed for the ring no. 0, layer 1 (figure 4.2) is 0.00028 mm^{-1}, that is 1.8 times less than the curvature (0.0005 mm^{-1}) used in the reconstruction. The explanation is that the change of the hit coordinates also changes the fitted track. This results in decreasing the residuals in the favour of fake hit (see fig. 4.4) - dotted line is original track, the solid one is the changed track). So if we want to get a value of a real curvature from the fit, we have to use 1.8 as a fudge factor.

However, the matter is a bit more complicated. Figure 4.3 shows the z residues as a function of local y for all the rings in layer 1. There is a significant decline in size of fitted bow, although the physical bow is same for all the modules in that layer. The probable reason, why this happens, is different θ for different rings, while the direction of shifting of hit remains the same. So in the ring 0 the hit is shifted in a direction of a track (fig. 4.5 A) causing minimal change in that track, while in the ring 6 (fig. 4.5 B) the hit is shifted perpendicular to the track, resulting in bigger change of the track.

To determine an exact size of this effect, we should calculate (at least) the first derivation of fitting function (that one which is used by Athena algorithm) in global r direction. That is, however, too complicated for this function cannot be written in an analytical form. Instead, the above mentioned effect was expected to be linear for small bows and the from the fitted tracks we determined the *fudge factors* . This is described in greater detail at section 4.3.4. Final test on random rings (section 4.3.5) showed, that this approach is reasonably precise for big numbers of fitted tracks passing through particular module.

4.3.3 ROOT macro for making plots from Athena ntuple

Because none of the values used in making plots at figures 4.2 and 4.3 is contained in the ntuple (for complete documentation see [24]), they had to be calculated using basic trigonometry. Angle ϕ and the $r-\phi$ residue can be collected from the ntuple, so

$$l = x \cos\phi, \tag{4.2}$$

where l is $x-y$ residue (as in fig. 4.1) and x is $r-\phi$ residue. Furthermore, we can calculate z residue from

$$z = l \operatorname{cotg}\theta = x \cos\phi \operatorname{cotg}\theta, \tag{4.3}$$

where z is the value of z residue.

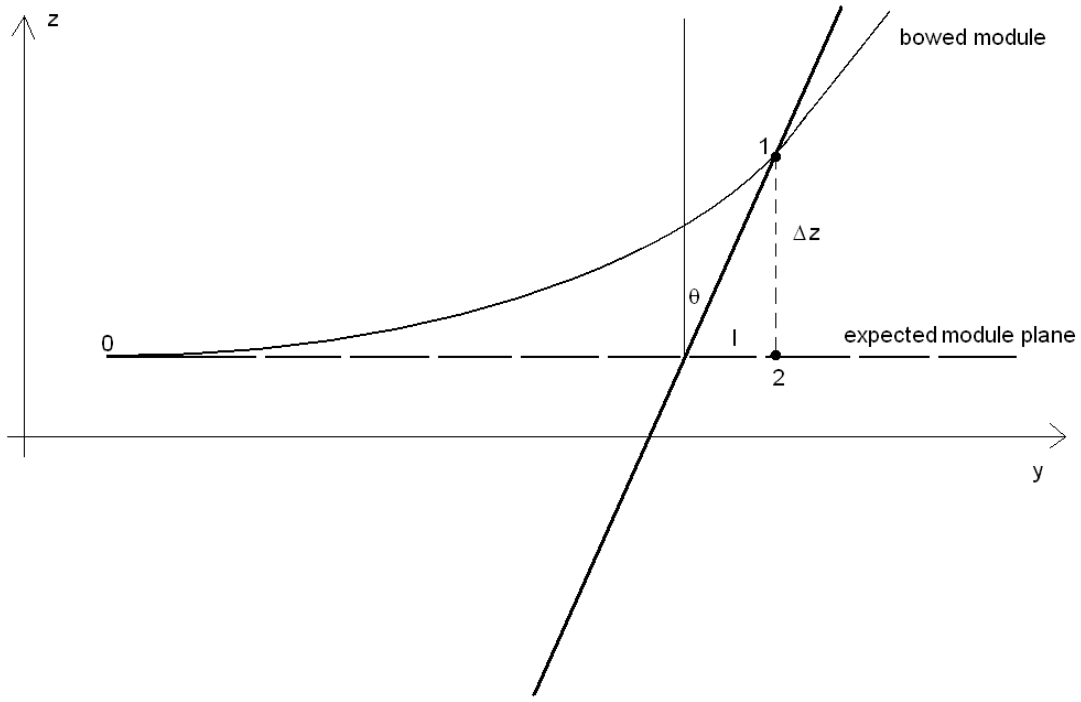

Figure 4.1: Effect of the bow

Also the value of the local y coordinate of the hit is not directly available but must be calculated by subtracting the global z coordinate of hit and the global z coordinate of the center of the module.

The ROOT macro consists of four C++ source files that can be found in a directory (accessible for example from LXPLUS)

`/afs/cern.ch/user/j/jez/public/bows/`

There are three main functions used to make a plot. The first one is `Modules (int DetType, int Layer, int Ring, int Side,string Output)`. This function at first determines how many events there are in the ntuple and creates an pointer to histogram. Then it is browsing through all the events using functions `Search(int DetType, int Layer, int Ring, int Event)` and `FillHist (int module, int event)`. `Search` gets one particular event and looks if during this

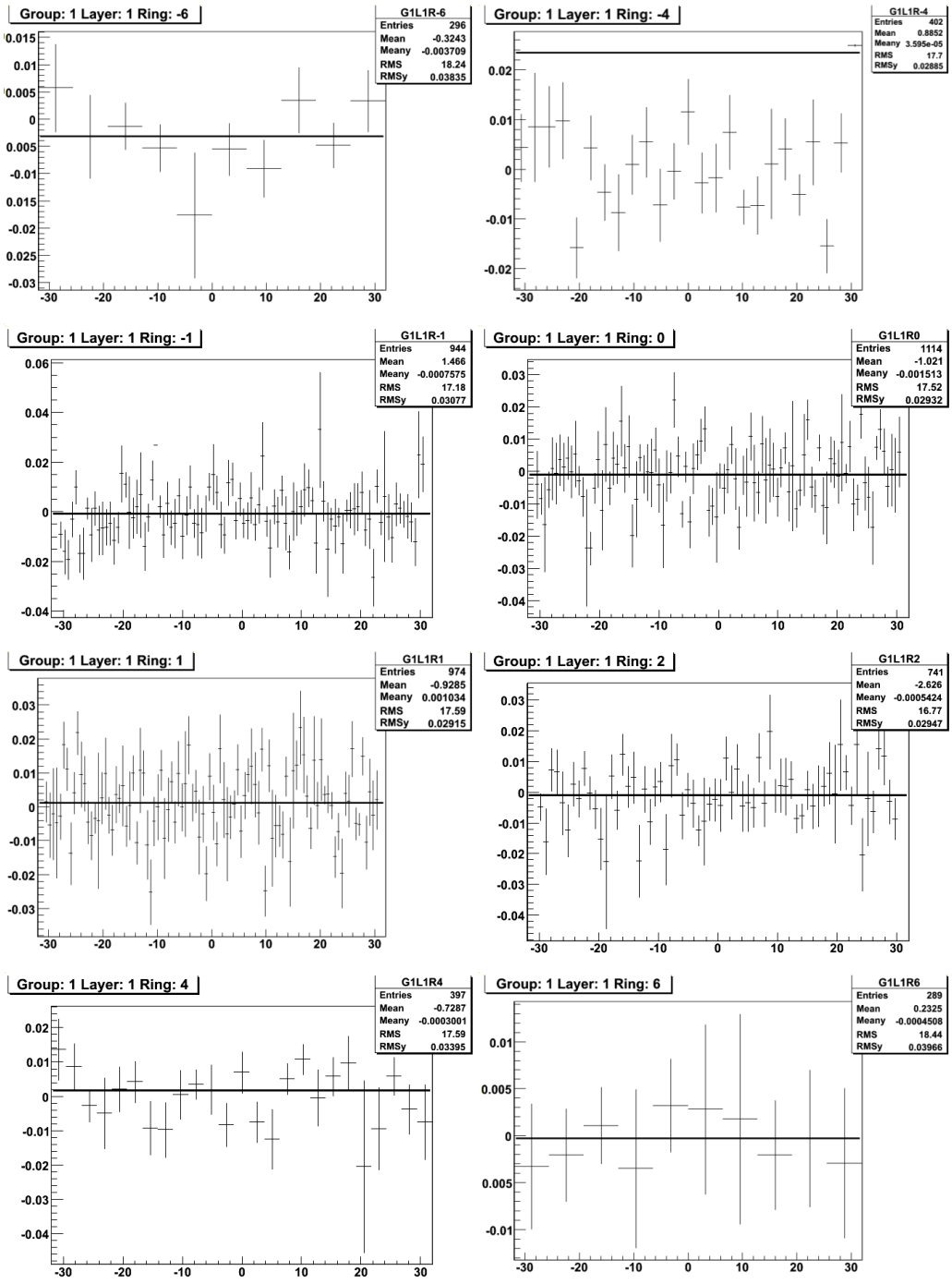

Figure 4.2: Modules without bows - plots of z residues as a function of local y

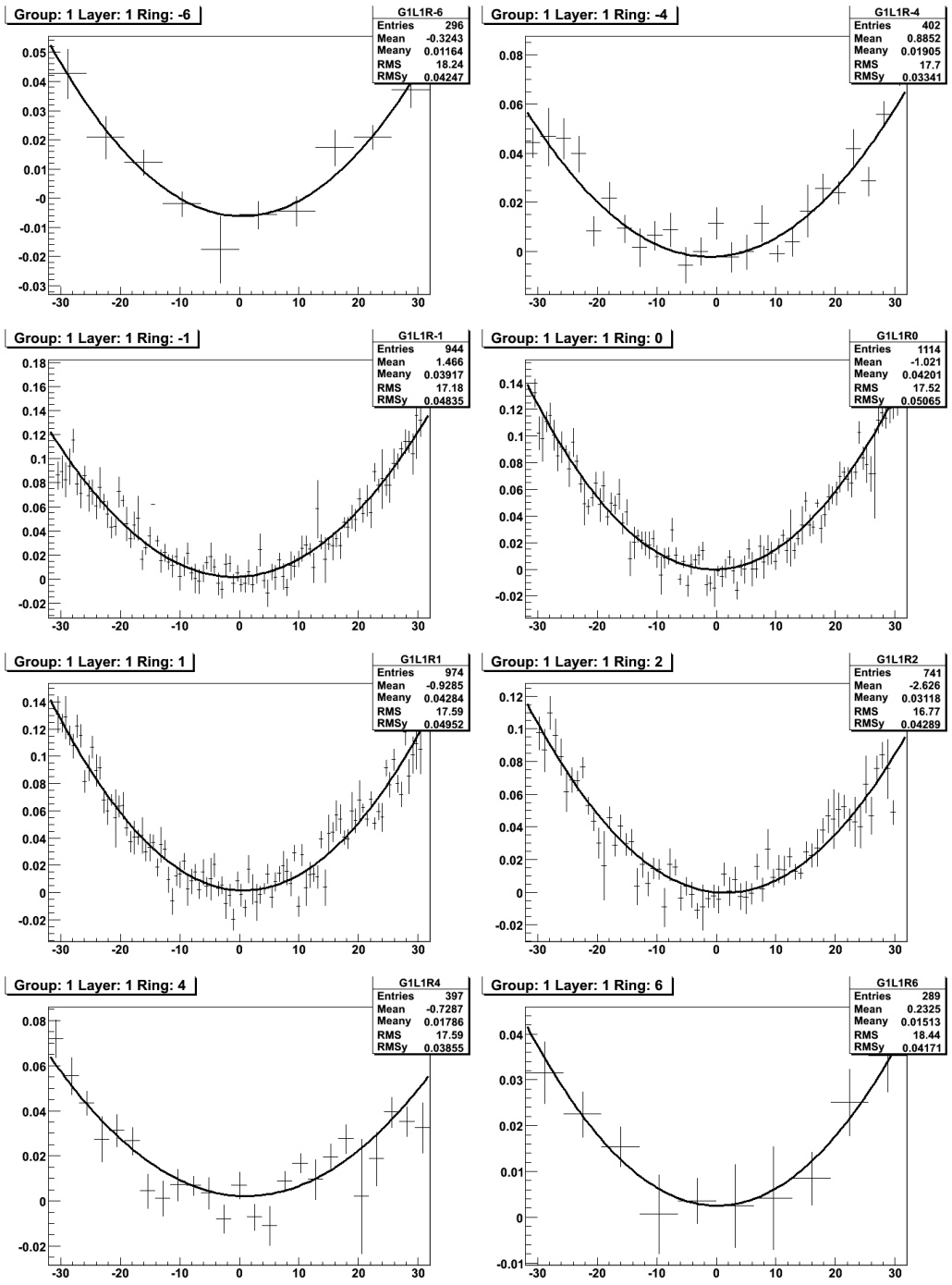

Figure 4.3: Modules with the bow of a size of 0.0005 mm^{-1}

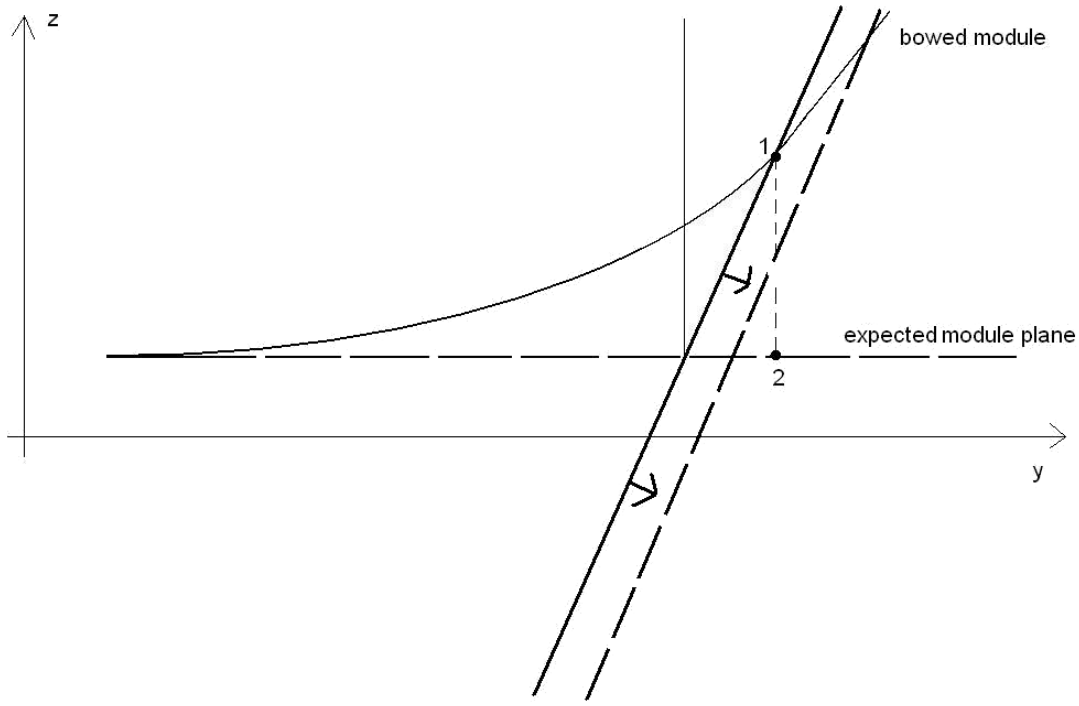

Figure 4.4: Change of the fitted track

event the muon passed through some module of given layer and ring and returns the order of such a module in that event (e.g. muon passes through 12 modules and the second of them lies in the desired layer and ring). In case muon goes through neighboring modules in the same ring and layer (the modules slightly overlap), the returned number is negative and its absolute value is the order of the first module muon passed through. `FillHist` is an "executive" function. It receives the number of event and the order of module in particular event (e.g. 2nd in the event number 127) so it can collect all necessary data from ntuple, calculate z residue according to (4.3) and place it into histogram. Finished histogram is finally written into ROOT file by function `Modules`. Next task of `Modules` is to calculate the quadratic fit of histogram values. The quadratic coefficient is called *bow qualificator* and it is proportional to the size of the bow. The fudge factor is the coefficient of proportionality.

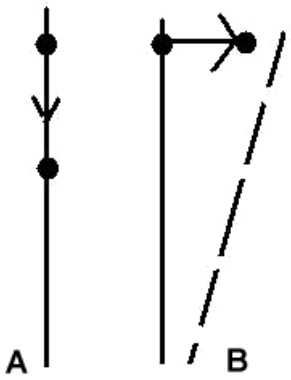

Figure 4.5: Changing of the fitted track at different rings

Therefore in the end the ROOT macro calculates the real curvature and print the resulting number into a text file. To get a set of histograms in one file (each of them corresponds to one ring and layer), function `Modules` is run in a cycle by unnamed ROOT script `Master.c`.

4.3.4 Determination of fudge factors

The *fudge factors* tell us the relation between the module's bow and the effect it produces as a consequence. As was mentioned above, the standard procedures do not work optimally - the same size of bow produces different change in resolution according to the module position. Therefore we introduced fudge factors as an geometrical correction. In this particular case, the smallest correction is needed in the central rings and the size of correction grows with η.

Practical way to determine fudge factors is to simulate different bows and find the correlation between the *bow qualificator* (calculated from the plot) and the bow used in simulation. Because of the forward-backward symmetry, only rings from 0 to 6 were used for determination of the fudge factors. Note that using fudge factors determined in this way gives reasonable results also in opposite hemisphere: i.e. at rings from -1 to -6.

The first task was to find a fudge constant for each ring and layer, independently on the size of the bow. Results for different bows (curvatures $5 \cdot 10^{-4}$ mm^{-1}, $4 \cdot 10^{-4}$ mm^{-1} and $2 \cdot 10^{-4}$ mm^{-1}) and layers could be found in the table 4.1. It shows that there is no universal fudge factor applicable for each ring and bow, but

on the other hand, for most of the rings a fudge factor can be found with error less than 10 % for bows between 0.0005 and 0.0002 mm^{-1}.

However, in outer rings with low statistics the fluctuations are bigger, so the fudge factors are more unsure and imprecise. In the last column of tab. 4.1, there is the number of tracks which were used to create the histograms (some of them are at fig. 4.3).

These fudge factors were stored in ROOT macro (variables `fudgeX`, where X is 0, 1 or 2), so it could calculate physical curvatures. At the rings -6, -5, 5, 6 of the layer 0 it was impossible to determine one fudge factor - due to the extremely low statistics, the corresponding macro failed to give any usable results. Thus, a factor of 1.0 was used instead. In this cases the first iteration is quite different from the real value of bow. Nevertheless, after a few iterations we would get reasonable values. Last remark is that the final precision is directly related to the robustness of the statistics and therefore the size of fluctuations.

4.3.5 Determining the bows by iterations

Important test of the ROOT macro was the calculation of the random bow size from the reconstructed tracks. After that the values of bow were used for recalculation of the tracks by Athena reconstruction algorithm. As a result we get a new set of bows which are used as an input in the next step of the iterative procedure. If everything is correct, than all bows should converge to stable values.

To perform this calculation, Athena *job option file* was set to produce an ntuple with parameters of tracks reconstructed using random bow value at each pixel module - this situation is indeed expected to occur in the detector. ROOT macro applied on such ntuple determined the size of bows using plots of z residuals and fudge matrix, as described above. The calculated values of bows were subtracted from the original bows (that ones used by Athena simulation) and obtained difference served as an input for Athena to reconstruct track again with the new parameters. Then the previous steps were iteratively repeated.

Results from that iteration are in table 4.2. The first column is the size of original bows, which were used by Athena simulation. In the second, third and fourth column there is what remained after first, second and third correction done by ROOT macro. The same information presented in another way is in table 4.3 where there are relative changes (with respect to the previous iteration as well as complete change - the fourth column). Last column shows the number of events which was used in reconstruction. Note that only typical representatives are shown.

We can see that practically for all "big" bows (i.e. with curvature bigger than

Table 4.1: Fudge factors

Layer/no. of ring	0.0005 mm^{-1}	0.0004 mm^{-1}	0.0002 mm^{-1}	hits
0/0	3.47	3.54	3.92	1664
0/1	3.52	3.53	3.55	1377
0/2	5.10	5.23	5.88	900
0/3	7.48	7.44	7.27	594
0/4	10.35	10.17	9.41	402
0/5	N/A	N/A	N/A	236
0/6	N/A	N/A	N/A	51
1/0	1.77	1.78	1.82	1114
1/1	1.88	1.88	1.90	974
1/2	2.39	2.37	2.33	741
1/3	3.36	3.39	3.53	529
1/4	4.29	4.24	4.03	397
1/5	5.10	5.12	5.21	354
1/6	6.49	6.78	8.94	289
2/0	1.61	1.61	1.64	825
2/1	1.74	1.76	1.85	768
2/2	1.86	1.84	1.73	646
2/3	2.75	2.84	2.96	470
2/4	4.09	4.25	5.53	367
2/5	5.18	5.33	6.27	314
2/6	5.07	5.17	5.70	283

0.0001 mm^{-1}) the correction worked properly. It converged quickly in the central rings with better determined fudge factors. The outer rings show that lack of hits (low statistics) makes this method of determination bows difficult.

Another phenomenon we can observe here is the bow low threshold of about 0.00009 mm^{-1} under which the method is also ineffective. The reason is that such a small bow is comparable to statistical fluctuations and not excluded that also due to problems with precision used. This feature is demonstrated at fig. 4.2 there are plots made by ROOT macro for ntuple with no bows - we can see that although the RMS is zero, the individual values are quite different from zero.

4.3.6 Improvement with growing statistics

After the close up the physical access to the detectors will not be possible and also during the accelerator shut-down the access will be very limited. Mathematical and software tools are powerful means for determination of individual sensing units (modules, sensors, layers, etc.). The obtained precision depends on number of factors, data statistics in one of most important. Here we demonstrate how convergence of the used method improves with statistics.

For quantitative verification of effect of statistics we analyzed two data sets: *low statistics* - 12 000 events (it is the same data as we used in previous sections) and *high statistics* - 110 000 single muon events. Comparison of the results from these two data sets is in the table 4.4, which presents the outcome in similar fashion as table 4.3, i.e. by calculation of relative changes.

Table 4.4 shows that in most cases the procedure significantly better converges to expected results. Similar effect can be observed also from table 4.3 where the iteration results (for sample *low statistics*) are shown with explicit indication of used statistics (last column).

It is obvious that fudge factor is more precisely determined using higher statistics. However, for more straightforward demonstration of the role of statistics, we used the same fudge factors in both data samples.

In general we can say that with growing statistics nearly all divergences (i.e. when the ROOT macro actually increases the size of bow) vanished and most of the bow iteration corrections decrease under the curvature of 0.0001 mm^{-1} during a few iterations (their effect on tracking performance is thus comparable or lower than that one originating from the intrinsic resolution of pixel modules). Nevertheless in some cases we can observe the fact, that the convergence is slower for higher statistics than for the lower. This is probably due to not optimal starting values of the fudge factors.

Table 4.2: Changing of curvatures through iterations (in mm^{-1})

layer/no. of ring	start	1st iteration	2nd iteration	3rd iteration
0/-6	-5,149E-05	1,074E-04	1,466E-04	1,505E-04
0/-3	1,604E-04	2,184E-05	-1,287E-05	-4,943E-05
0/-1	3,885E-04	4,297E-05	5,202E-06	3,804E-06
0/0	-2,444E-04	-1,174E-04	-6,807E-05	-5,525E-05
0/1	1,836E-05	2,078E-05	1,232E-05	9,392E-06
0/2	1,546E-05	-3,757E-05	-7,433E-05	-8,123E-05
0/3	-9,882E-06	5,303E-05	4,628E-05	4,385E-05
0/6	8,194E-05	8,520E-06	-4,296E-06	-5,796E-06
1/-6	2,868E-04	3,146E-04	3,343E-04	3,556E-04
1/-4	-2,764E-04	-1,389E-05	1,356E-04	1,633E-04
1/-1	-2,750E-05	-3,126E-05	-2,091E-05	-2,036E-05
1/0	-4,370E-04	-2,356E-05	-9,380E-07	-2,626E-06
1/1	-3,877E-04	-9,543E-06	-3,037E-06	-2,739E-06
1/2	1,274E-05	3,968E-05	1,619E-05	1,362E-05
1/4	2,078E-04	6,082E-05	4,010E-05	3,284E-05
1/6	-1,091E-04	-1,988E-04	-1,946E-04	-1,861E-04
2/-6	1,007E-04	3,984E-05	1,186E-05	-4,332E-06
2/-3	-2,927E-04	-2,545E-05	4,310E-05	5,305E-05
2/-1	2,931E-04	2,468E-05	3,713E-05	3,050E-05
2/0	1,081E-04	2,255E-05	-3,969E-06	-5,527E-06
2/1	-8,271E-05	-2,640E-05	-2,373E-05	-2,243E-05
2/2	-3,212E-04	4,255E-05	2,534E-05	2,459E-05
2/4	-3,350E-04	-4,328E-04	-4,516E-04	-4,594E-04
2/6	4,169E-04	6,914E-05	-2,286E-05	-4,492E-05

Table 4.3: Relative changes during iterations

layer/ no. of ring	after 1st iteration	after 2nd iteration	after 3rd iteration	complete relative change	no. of hits
0/-6	-208,65%	136,42%	102,70%	-292,34%	51
0/-3	13,61%	-58,95%	384,03%	-30,82%	574
0/-1	11,06%	12,11%	73,13%	0,98%	1334
0/0	48,04%	57,98%	81,17%	22,61%	1664
0/1	113,18%	59,28%	76,26%	51,16%	1377
0/2	-243,05%	197,83%	109,29%	-525,49%	900
0/3	-536,69%	87,27%	94,75%	-443,77%	594
0/6	10,40%	-50,42%	134,93%	-7,07%	51
1/-6	109,69%	106,29%	106,35%	123,99%	296
1/-4	5,03%	-976,12%	120,40%	-59,08%	402
1/-1	113,66%	66,89%	97,36%	74,02%	944
1/0	5,39%	3,98%	279,98%	0,60%	1114
1/1	2,46%	31,82%	90,19%	0,71%	974
1/2	311,45%	40,80%	84,12%	106,90%	741
1/4	29,27%	65,93%	81,90%	15,80%	397
1/6	182,28%	97,87%	95,64%	170,61%	289
2/-6	39,56%	29,76%	-36,54%	-4,30%	274
2/-3	8,70%	-169,35%	123,08%	-18,13%	469
2/-1	8,42%	150,47%	82,15%	10,41%	778
2/0	20,87%	-17,60%	139,26%	-5,11%	825
2/1	31,92%	89,91%	94,51%	27,12%	768
2/2	-13,25%	59,55%	97,05%	-7,66%	646
2/4	129,22%	104,34%	101,72%	137,15%	367
2/6	16,58%	-33,07%	196,45%	-10,77%	283

Table 4.4: Effect of higher statistics on the quality of the bow determination

layer/ no. of ring	initial bow (mm^{-1})	after 1st iteration (low stats)	after 1st iteration (high stats)	after 3rd iteration (low stats)	after 3rd iteration (high stats)
0/-6	-5,149E-05	-208,65%	-55,91%	-292,34%	-61,30%
0/-3	1,604E-04	13,61%	29,93%	-30,82%	-10,92%
0/-1	3,885E-04	11,06%	21,18%	0,98%	-2,98%
0/0	-2,444E-04	48,04%	28,15%	22,61%	-2,82%
0/1	1,836E-05	113,18%	4,70%	51,16%	2,45%
0/2	1,546E-05	-243,05%	110,80%	-525,49%	-43,80%
0/3	-9,882E-06	-536,69%	-476,06%	-443,77%	189,58%
0/6	8,194E-05	10,40%	-93,76%	-7,07%	-88,74%
1/-6	2,868E-04	109,69%	39,61%	123,99%	-15,62%
1/-4	-2,764E-04	5,03%	29,82%	-59,08%	-7,17%
1/-1	-2,750E-05	113,66%	-90,55%	74,02%	4,49%
1/0	-4,370E-04	5,39%	5,04%	0,60%	-0,54%
1/1	-3,877E-04	2,46%	0,46%	0,71%	-0,12%
1/2	1,274E-05	311,45%	177,89%	106,90%	-34,18%
1/4	2,078E-04	29,27%	20,99%	15,80%	-9,06%
1/6	-1,091E-04	182,28%	106,28%	170,61%	-60,68%
2/-6	1,007E-04	39,56%	70,85%	-4,30%	-34,32%
2/-3	-2,927E-04	8,70%	25,90%	-18,13%	-3,80%
2/-1	2,931E-04	8,42%	6,19%	10,41%	-1,32%
2/0	1,081E-04	20,87%	34,11%	-5,11%	2,85%
2/1	-8,271E-05	31,92%	3,70%	27,12%	0,77%
2/2	-3,212E-04	-13,25%	-5,18%	-7,66%	-0,20%
2/4	-3,350E-04	129,22%	58,56%	137,15%	-21,74%
2/6	4,169E-04	16,58%	43,34%	-10,77%	-13,16%

Chapter 5

Thesis Summary

The first chapter of this thesis presents the basic ideas of the Standard Model. This theory turned out to be one of the greatest scientific achievements of the twentieth century: the experiments in the last twenty years (LEP, Tevatron) verified its predictions with the precision better than one per cent. However, some of its predictions are not confirmed yet: one of the principal questions is the existence of Higgs boson, the particle which plays crucial role in the mechanism that solves the problem of the spontaneous symmetry breaking of the electroweak Lagrangian.

The search for Higgs boson is one of the main motivations why the LHC is being built. Also, as discussed in section 1.5.5, the number of the free parameters of the Standard Model (24 - cf. [1]) indicates that it is not the final theory of the particle world, but rather an effective approximation for lower energy scales ($\lesssim 1$ TeV). The LHC would help us to explore the physics beyond the Standard Model.

The second chapter describes the CERN experimental complex and the LHC in particular. It reveals the challenges the constructors of the LHC have to deal with and also briefly describes the main physics features to be studied with the help of this machine. The second chapter also briefly presents the five experiments which explore the LHC physics.

The third and fourth chapter are devoted to one of this experiments - ATLAS. We described the main directions of research at ATLAS as well as the detector apparatus. We showed that Inner Detector is crucial for tracking and particle identification, therefore we try to achieve the best possible resolution.

The most precise part of the Inner Detector are pixel modules. Their intrinsic resolution is ~ 14 μm, however this value can be degraded a lot due to module misalignment and shape distortions. The effects of misalignment will not be negligible from the beginning, on the contrary, the expected degradation is from 25 % to

100 %, however it will still allow us to see tracks and therefore calibrate the Inner Detector for precision measurements.

The other of the major sources of the deterioration of the tracking resolution are module shape distortions. According to the initial surveys they take form of a longitudinal bow with a curvature ~ 0.0002 mm^{-1}. This means, that the displacement from the nominal planes is c. 100 μm at the end of the modules (cf. (4.1)). The present study demonstrates the procedure of determination of bow using fitted tracks. As an input in the iterative calculation serves approximative value of bow obtained by the mechanical survey of module shapes before installation.

We used the method of the successive approximations: we calculated the size of the bow, subtracted effects of such a bow from the reconstruction data and determined the size of the bow again. This was repeated twice. Results showed that the improvement in the resolution is highly dependent on the number of events. Tables 4.2 and 4.3 show, that to achieve precision comparable with the intrinsic resolution of pixels (~ 15 μm), we need c. 500 events per module. For the statistics of 12 000 events, this was achieved in the central region of pixel barrel: rings -1 and 1 in the layer 0 and rings from -2 to 2 in other two layers.

When we increased the total number of events to 110 000, we observed that c. 4000 hits per module (6000 in the layer 0) leads to negligible resolution degradation (~ 1 μm). As a result of this analysis we found that 4.7×10^6 single muon events are sufficient for alignment in case of a uniform hit population.

In the realistic geometric detector configuration, the effects of bows are smaller at the end of the barrels (see figure 4.3) - they are approximately halved there. If we relax our demands on resolution to ~ 30 - 40 μm, tables 4.2 and 4.3 tell us that we would need c. 300 events per module. This means 2.9×10^6 single muon events altogether. Such numbers are easily obtainable quite soon after ATLAS to be put into operation. High statistics of experimental data implicates re-coding of not enough efficient present macro to reach data rate requirement.

Table 4.4 presents direct comparison of low (12 000) and high (110 000) statistics. It also shows several general characteristics of this method:

- The speed of convergence depends on the initial value and the best results are achieved for bows with the size ~ 0.0002 mm^{-1}. On the other hand, this method does not converge for the bows below certain threshold. For low statistics it is about 0.0001 mm^{-1}, but for the high statistics the low threshold is more than 10 times smaller, corresponding to the deterioration in resolution $\sim$ 1-2 μm.

- The quality of the bow determination is also dependent on the position of the

module. The leading effect plays here the spatial coverage of given detection module, which is directly related to the number of detected hits. Further influence comes from the particle momentum spectra and the magnetic field.

Similar to the previous case (pixel and SCT misalignment), it will take just a few days of data taking to achieve a reasonable precision, but much longer time is needed to understand the systematics (represented in this case by fudge factors - tab. 4.1) of pixel module bows. The results from the section 4.3.6 (especially table 4.4) signals that the very concept of fudge factors needs revision, as it is not fully consistent - there were several groups of modules where the higher statistics decreased the speed of convergence. The probable reason is that the initial results for fudge factors (tab. 4.1) show some non-linearities - they could be caused by low statistics, but (more probably) by the non-linear effect of shape distortions. Possible solution would be bow dependent fudge factors. Detailed study of the reconstruction algorithm is therefore inevitable.

The results described in the last part of this thesis were presented on ATLAS Collaboration meetings - see [28] and [29].

To sum up, the approach described in this chapter will help us to achieve designed precision of the Inner Detector, which is crucial for charge particle momentum measurement. Obtained data are essential for offline analysis and thus allow us precise study of the outcome of the proton-proton collisions, which is the target of the ATLAS physics programme.

Appendix A

Glossary of ATLAS/High energy physics terms

ATLAS global coordinate system is cylindrical. The z axis points in the direction of the beam, R is the distance from the center and ϕ is a polar angle. It is measured from positive x axis (see below) clockwise. The plane perpendicular to the beam direction is sometimes called $R - \phi$ plane. There is also a global cartesian system, where x points to the center of the LHC ring, y going upwards and z pointing towards the Point 8.

ATLAS local coordinate system is cartesian. At given point (with a distance R from the beam axis), the local x and y axes are in a plane which is tangent to the surface of cylinder around the beam axis with radius R. Local y axis points in the direction of the beam (or global z), local x points in the direction of global ϕ. Local z axis then points out of the beam axis, i.e. in the direction of global R. Azimuthal angle θ is measured with respect to the local z axis.

Athena is a control software framework and it is a concrete implementation of an underlying architecture called Gaudi. It is a skeleton of an application into which developers can plug their code. It provides common functionality and communications between different components, thus encouraging the common approach. The user's guide and the documentation can be found at [19].

Barrel is a central area of ATLAS, where the components (detectors, calorimeters, magnets, etc.) are placed in a cylindrical fashion around the central axis.

Branching ratio for a particular decay is the ratio between the decay rates of individual decay modes for the decay and the total decay rate.

Endcaps is an overall term for area on both ends of ATLAS. Components are mounted on a disks perpendicular to the central axis there.

Hit is a point where particle passes through the detector.

iPatRec is one of the reconstruction algorithms. Track finding is defined by calorimeter clusters or muon tracks starting in the silicon detectors. It adds TRT for the best resolution.

Jets are group of highly collimated hadrons which result from the hadronization of partons (quark and gluons) that were produced in hard collisions. It is a consequence of quark confinement.

Ntuple is a set of information about an experiment. It contains the position of all hits of all events that happened during the particular experiment/simulation. Ntuple also harbours the parameters of reconstructed tracks - e.g. direction in which they pass through particular module, or their momenta. However, content of a particular ntuple depends on its purpose - for instance the ntuples used in this study contained also position and characteristics of all participating pixel and SCT modules. Nowadays ntuples are usually stored in the form of ROOT files.

Pseudorapidity is defined as

$$\eta = -\ln \mathrm{tg}\frac{\theta}{2}$$

It is a handy variable used to approximate the rapidity in case we do not know the mass and the momentum of the particle. We can get it from the rapidity

$$y = \frac{1}{2}\ln\frac{1+\beta\cos\theta}{1-\beta\cos\theta}$$

when we set $\beta = 1$. At LHC the particles will collide with more than 99.999 % of the speed of light, so we can use this approximation.

ROOT is an object-oriented framework aimed at solving the data analysis challenges of high energy physics. It has a wide variety of objects like histograms, fitting, etc. so the physicists can analyze the data with only little knowledge of C++. It also encourages the common approach and reusability of analytical macros. Complete (and very well written) documentation is available at [20]

Transition radiation is produced when a relativistic particle crosses the interface of two media of different dielectric constants. The emitted radiation is a homogenous difference between the solutions of Maxwell's equations for fields generated by movement of particle in each medium separately. The intensity of radiation is proportional to the particle energy $E = m\gamma$. This phenomenon offer a possibility of identification of particles at highly relativistic energies, where Cherenkov radiation is no longer useful for particle discrimination.

Vertex is other name for interaction point, i.e. a point where the number and/or momenta of interacting particles have changed.

xKalman is one of the reconstruction algorithms. Track finding and fitting starts from the TRT detector, then it extends to the precision layers of pixel and SCT detectors.

Bibliography

[1] J. Hořejší, *Fundamentals of Electroweak Theory*, Karolinum Press, 2002

[2] L. H. Ryder, *Quantum Field Theory*, 2nd edition, Cambridge University Press, 1996

[3] J. Chýla, *Quarks, partons and Quantum Chromodynamics*, lecture notes, `http://www-hep2.fzu.cz/Theory/notes/text.pdf`

[4] S. F. Novaes, *Standard model: An introduction*, 10th Jorge Andre Swieca Summer School: Particle and Fields, Sao Paulo, Brazil, 31/1 - 12/2 1999, hep-ph/0001283

[5] S. Eidelman *et al.*, Phys. Lett. **B592**, 1 (2004) and 2005 partial update for the 2006 edition available on the PDG WWW pages, `http://pdg.lbl.gov/`

[6] J. R. Christman, *SU(3) and the Quark Model*, project PHYSNET, MISN-0-282, `http://www.physnet.org`

[7] J. R. Christman, *The Strong Interaction*, project PHYSNET, MISN-0-280, `http://www.physnet.org`

[8] ATLAS collaboration, *ATLAS Technical Proposal for a General-Purpose pp Experiment at the Large Hadron Collider at CERN*, 2nd edition, CERN, 1994

[9] CERN public pages, section "How do physicist study particles", `http://public.web.cern.ch/Public/Content/Chapters/AboutCERN/HowStudyPrtcles/HowStudyPrtcles-en.html`

[10] LHC machine Outreach, `http://lhc-machine-outreach.web.cern.ch/lhc-machine-outreach/`

[11] ATLAS experiment public pages, http://atlas.ch/

[12] G. V. Velev, *Top Mass Measurements at the Tevatron Run II*, hep-ex/0510007

[13] O. S. Brüning *et al.*, *LHC Design Report v.1*, CERN-2004-003-V-1, http://ab-div.web.cern.ch/ab-div/Publications/LHC-DesignReport.html

[14] N. V. Krasnikov, V. A. Matveev, *Physics at LHC*, Phys.Part.Nucl.28:441-470, 1997, hep-ph/9703204

[15] CMS Outreach, http://cmsinfo.cern.ch/

[16] ALICE experiment: Panorama of ALICE, http://aliceinfo.cern.ch/Public/panorama/

[17] LHCb public pages, http://lhcb-new.web.cern.ch/

[18] TOTEM experiment homepage, http://totem.web.cern.ch/Totem/

[19] ATLAS computing wiki page: ATLAS workbook, https://uimon.cern.ch/twiki/bin/view/Atlas/WorkBookAthenaFramework

[20] M. Goto *et al.*, *ROOT User's Guide v5.08*, http://root.cern.ch/root/doc/RootDoc.html

[21] V. Drollinger, *Review of Higgs Physics at the LHC*, hep-ph/0405026

[22] R. K. Bock, A. Vasilescu, *Particle Detector Briefbook*, http://rkb.home.cern.ch/rkb/PH14pp/node1.html

[23] R. Hawkings, *Module distortion in the SCT and pixel detectors and their effect on tracking resolution*, ATLAS internal note on August 16th, 2005

[24] R. Hawkings, *iPatRec Ntuples for Tracking Alignment Studies*, 2nd version, 2002

[25] R. Hawkings, P. Jež, *Initial Alignment of the ATLAS SCT and Pixel Detectors and Its Effect on Track-finding*, ATLAS internal note on August 23rd, 2005 (revised version)

[26] S. Snow, A. Weidberg, *The effects of inner detector misalignment on track resolution*, ATLAS internal note, INDET-97-160

[27] J. Blank, P. Exner, M. Havlíček, *Hilbert-Space Operators in Quantum Physics*, American Institute of Physics, 1994

[28] P. Jež, *Determination of the bow for the pixel modules using fitted tracks*, presentation held at ID week, CERN, 26/9/05, `http://agenda.cern.ch/fullAgenda.php?ida=a052086#2005-09-26`

[29] R. Hawkings, P. Jež, *Determination of the bow for the pixel modules*, presentation held at ID week, CERN, 13/12/05, `http://agenda.cern.ch/fullAgenda.php?ida=a056637#2005-12-13`